Research Square

Preprints are preliminary reports that have not undergone peer review.
They should not be considered conclusive, used to inform clinical practice,
or referenced by the media as validated information.

P2RX7 programs checkpoint-responsive exhausted CD8+ T cell states through a KLF3 metabolic circuit

Henrique Borges da Silva

hbsilva8787@gmail.com

Department of Immunology, Mayo Clinic College of Medicine and Science

Caio Salgado

Mayo Clinic Arizona https://orcid.org/0000-0002-4423-6723

Leticia Kogachi

Department of Immunology, Mayo Clinic College of Medicine and Science

Guilherme Souza-Silva

Department of Immunology, Mayo Clinic College of Medicine and Science

Igor Santiago-Carvalho

Department of Immunology, Mayo Clinic College of Medicine and Science

Haiguang Wang

University of Minnesota Medical School https://orcid.org/0000-0001-5403-9179

Changwei Peng

Harvard Medical School https://orcid.org/0000-0002-0710-9573

Bruna Macedo

Mayo Clinic Arizona https://orcid.org/0000-0001-6907-1630

Constantine Yerocostas

Department of Immunology, Mayo Clinic College of Medicine and Science

Jian Shen

Northwestern University https://orcid.org/0000-0001-8398-2318

Kexin Gai

Northwestern University Feinberg School of Medicine

Olivia Liseth

Mayo Clinic https://orcid.org/0000-0001-8916-0470

Angad Beniwal

Department of Immunology, Mayo Clinic College of Medicine and Science

Dustin Grief

Department of Hematology/Oncology, Mayo Clinic College of Medicine and Science

Nhan Tran

Division of Immunology and Microbiome, Translational Genomics Research Institute

Richard Vile

Mayo Clinic https://orcid.org/0000-0003-2192-9372

Bryan Husta

Department of Pulmonary and Critical Care Medicine, Mayo Clinic College of Medicine and Science

John Copland

Department of Cancer Biology, Mayo Clinic College of Medicine and Science

J. Justin Milner

University of North Carolina https://orcid.org/0000-0002-0752-2130

Stephen Jameson

University of Minnesota Medical School https://orcid.org/0000-0001-9137-1146

Weiguo Cui

Northwestern University Feinberg School of Medicine https://orcid.org/0000-0003-1562-9218

Article

Keywords:

Posted Date: November 10th, 2026

DOI: https://doi.org/10.21203/rs.3.rs-10375256/v1

License: This work is licensed under a Creative Commons Attribution 4.0 International License. Read Full License

Additional Declarations: Yes there is potential Competing Interest. Bryan Husta is a consultant to Intuitive Surgical. All other authors declare that they have no competing interests.

P2RX7 programs checkpoint-responsive exhausted CD8$^+$ T cell states through a KLF3 metabolic circuit

Caio L. Salgado,[1] Leticia Kogachi,[1] Guilherme A. Souza-Silva,[1,2] Igor Santiago-Carvalho,[1]† Haiguang Wang,[3] Changwei Peng,[3]‡ Bruna G. Macedo,[1] Constantine Yerocostas,[1] Jian Shen,[4] Kexin Gai,[4] Olivia Liseth,[5] Angad Beniwal,[1] Dustin K. Grief,[6] Nhan L. Tran,[7] Richard Vile,[5] Bryan Husta,[8] John A. Copland,[9] J. Justin Milner,[10] Stephen C. Jameson,[3] Weiguo Cui,[4] Henrique Borges da Silva[1,11]*

Affiliations

[1]Department of Immunology, Mayo Clinic, Phoenix, AZ, United States.

[2]Department of Parasitology, Instituto de Ciencias Biomedicas, Universidade de Sao Paulo, Sao Paulo, Brazil.

[3]Center for Immunology, University of Minnesota, Minneapolis, MN, United States.

[4]Department of Pathology, Feinberg School of Medicine, Northwestern University, Chicago, IL, United States.

[5]Department of Immunology, Mayo Clinic, Rochester, MN, United States.

[6]Department of Hematology/Oncology, Mayo Clinic, Phoenix, AZ, United States.

[7]Division of Immunology and Microbiome, Translational Genomics Research Institute, Phoenix, AZ, United States.

[8]Department of Pulmonary and Critical Care Medicine, Mayo Clinic, Jacksonville, FL, United States.

[9]Department of Cancer Biology, Mayo Clinic, Jacksonville, FL, United States.

[10]Lineberger Comprehensive Cancer Center, University of North Carolina at Chapel Hill, Chapel Hill, NC, United States.

[11]Department of Cancer Biology, Mayo Clinic, Phoenix, AZ, United States.

*Corresponding author. Email: hbsilva8787@gmail.com.

†Present address: Department of Immunology, Instituto de Ciencias Biomedicas, Universidade de Sao Paulo, Sao Paulo, Brazil.

‡Present address: Department of Immunology & HMS Center for Immune Imaging, Harvard Medical School, Boston, MA, United States.

Abstract

Checkpoint-responsive exhausted $CD8^+$ T cells sustain immunity during chronic infection and cancer, but the tissue-derived signals that preserve these cells remain poorly defined. Here, we identify extracellular ATP sensing through P2RX7 as a microenvironmental circuit that maintains progenitor exhausted (T_{PEX}) and tissue-resident exhausted (TR_{TEX}) $CD8^+$ T cells. P2RX7 was enriched in T_{PEX} and TR_{TEX} cells and was required cell-intrinsically to preserve their abundance, diversity, and developmental competence during chronic viral infection. Loss of P2RX7 restricted early progenitor trajectories and induced mitochondrial dysfunction, lipid peroxidation, and terminal exhaustion-associated phenotypes. Mechanistically, P2RX7-dependent Ca^{2+} influx activated NFAT/AP-1 signaling, which induced KLF3 to promote mitochondrial fitness, subset development, and persistence of T_{PEX} and TR_{TEX} cells. P2RX7 also supported $CD8^+$ T cell expansion after PD-1 blockade, whereas pharmacologic P2RX7 activation enhanced antitumor immunity in preclinical models. These findings define an extracellular ATP-P2RX7-KLF3 program that couples tissue damage sensing to metabolic adaptation and persistence of checkpoint-responsive exhausted $CD8^+$ T cells.

Persistent antigen stimulation in chronic infection and cancer drives $CD8^+$ T cell exhaustion, a heterogeneous differentiation state marked by impaired effector function, inhibitory receptor expression, and altered transcriptional and epigenetic regulation[1–4]. Progenitor exhausted (T_{PEX}) cells retain self-renewal capacity and generate the proliferative burst that follows PD-1 blockade. Tissue-resident exhausted (TR_{TEX}) cells persist within inflamed tissues and tumors, are associated with responses to PD-1 blockade, and have been linked to local immune control[5–7]. By contrast, terminally exhausted subsets show limited durability. Although the transcription factors and chromatin states that define these subsets are increasingly well described[8–14], less is known about the tissue-derived signals that promote the development and persistence of therapeutically responsive exhausted $CD8^+$ T cell states during chronic antigen exposure.

Chronically inflamed tissues expose T cells to persistent TCR signaling, checkpoint ligands, metabolic constraint, and damage-associated signals[15–18]. Among these cues, extracellular ATP is released during infection, tumor growth, and tissue injury and is sensed by purinergic receptors, including P2RX7, a ligand-gated ion channel that promotes Ca^{2+} influx and downstream signaling[19–22]. Because extracellular ATP is enriched at sites of cell damage, antigen persistence, and tissue remodeling, it may provide spatial information that instructs local T cell adaptation rather than serving only as a generic inflammatory byproduct. In line with a role for extracellular ATP sensing in T cell adaptation, P2RX7 supports memory $CD8^+$ T cell metabolic fitness and cell survival[23–25]. However, whether extracellular ATP sensing actively shapes exhausted $CD8^+$ T cell fate under chronic antigen stimulation, rather than simply reflecting tissue damage or memory-associated biology, has remained unclear.

Here we identify P2RX7 as a microenvironmental sensor that preserves checkpoint-responsive exhausted $CD8^+$ T cell subsets. P2RX7 marks T_{PEX} and TR_{TEX} cells and is required cell intrinsically to maintain their function, diversity, and developmental competence across chronic viral infection and tumor models. Mechanistically, P2RX7-dependent Ca^{2+} signaling sustains NFAT/AP-1 activity and induces KLF3, which supports exhausted $CD8^+$ T cell mitochondrial fitness and restrains terminal dysfunction. Together, these findings define an extracellular ATP–P2RX7–KLF3 circuit that links tissue damage sensing to the persistence of therapeutically responsive exhausted $CD8^+$ T cell states.

Results

P2RX7 marks and maintains therapeutically responsive exhausted $CD8^+$ T cell states

We first asked whether P2RX7 identifies the exhausted $CD8^+$ T cell states most relevant to durable immunity during chronic antigen exposure. To map these states, we performed single-cell RNA sequencing (scRNA-seq) on antigen-specific P14 $CD8^+$ T cells isolated from LCMV Clone 13-infected mice at day 30 post-infection (**Fig. 1a**; gating strategy in **Extended Data Fig. 1**). UMAP clustering resolved populations corresponding to progenitor exhausted (T_{PEX}) and tissue-resident exhausted (TR_{TEX}) subsets. Both T_{PEX} and TR_{TEX} clusters were enriched for *P2rx7* mRNA compared with other exhausted or memory subsets, with strongest enrichment in T_{PEX} cells (**Fig. 1b,c**, **Extended Data Fig. 2a**, **Supplementary Table 1**). Flow cytometry confirmed increased P2RX7 expression in T_{PEX} and TR_{TEX} cells during chronic LCMV infection and in MC38 tumor-bearing mice (**Fig. 1d,e**). As previously reported[7,23–25], resident memory $CD8^+$ T cells from LCMV Armstrong-infected mice also expressed high P2RX7 levels

(**Extended Data Fig. 2b**). Thus, P2RX7 expression extends from memory and resident memory states into distinct exhausted progenitor and resident compartments generated during chronic antigen exposure.

We next tested whether P2RX7 was required to preserve these subsets *in vivo*. CD8-specific deletion of *P2rx7* in CD8-Cre *P2rx7*$^{fl/fl}$ mice reduced antigen-specific T_{PEX} and TR_{TEX} populations in spleen and liver during chronic infection (**Fig. 1f,g**; subset gating in **Extended Data Fig. 1**) and was associated with reduced viral control (**Fig. 1h**). Mixed adoptive transfer experiments demonstrated that this requirement was cell intrinsic: P2RX7-deficient P14 cells failed to efficiently generate and maintain T_{PEX} and TR_{TEX} cells in competitive settings (**Fig. 1i,j**), whereas terminal and effector exhausted subsets were less affected and NK-like exhausted $CD8^+$ T cells were increased[26]. Together, these data identify P2RX7 as a cell-intrinsic gatekeeper of the progenitor and resident exhausted $CD8^+$ T cell pools that sustain chronic antiviral immunity.

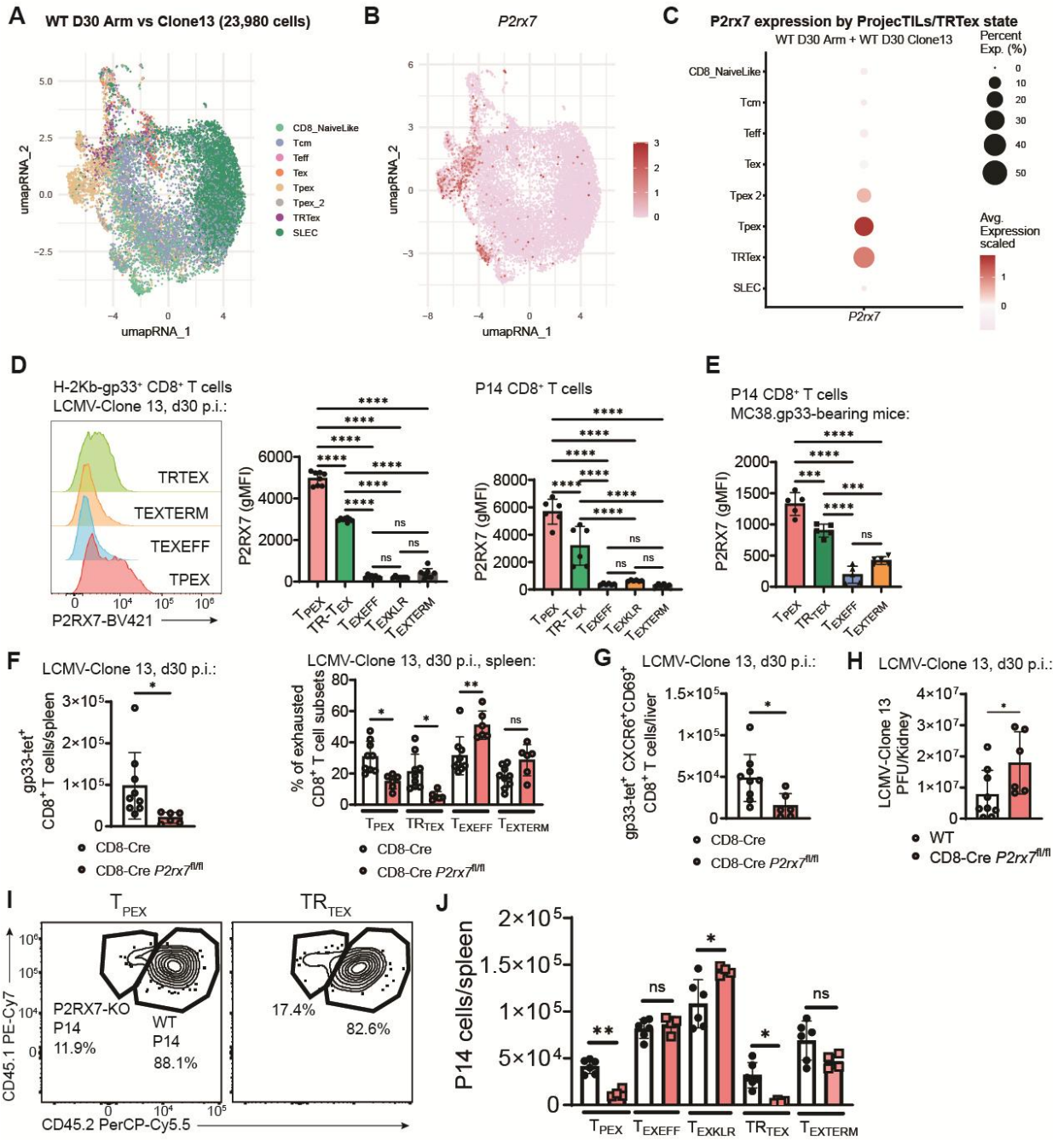


Fig. 1. P2RX7 marks and maintains T_{PEX} and TR_{TEX} cells during chronic antigen exposure. (a–c) P14 CD8⁺ T cells were sorted from LCMV-Armstrong- or LCMV-Clone 13-infected mice at day 30 post-infection (p.i.) and analyzed by scRNA-seq. UMAPs show annotated clusters and normalized *P2rx7* expression; bubble plot shows normalized *P2rx7* expression across clusters. **(d)** Representative histograms and gMFI of P2RX7 in exhausted CD8⁺ T cell subsets from LCMV-Clone 13-infected mice at day 30 p.i., measured in endogenous gp33-tetramer⁺ and transferred P14 cells. **(e)** P2RX7 gMFI in exhausted P14 subsets from MC38.gp33-bearing mice. **(f and g)** WT (CD8-Cre) and CD8-Cre *P2rx7*$^{fl/fl}$ mice were infected with LCMV-Clone 13, and gp33-tetramer⁺ CD8⁺ T cells were analyzed at day 30 p.i. Total splenic CD8⁺ T cell numbers, exhausted subset frequencies, and CXCR6⁺CD69⁺ liver CD8⁺ T cell numbers are shown. **(h)** LCMV-Clone 13 PFU in WT and CD8-Cre *P2rx7*$^{fl/fl}$ mice. **(i and j)** WT (CD45.1/2⁺) and P2RX7-KO (CD45.1⁺) P14 cells were co-transferred at a 1:1 ratio into LCMV-Clone 13-infected recipients. Representative plots and absolute numbers of splenic exhausted P14 subsets are shown. **(d–j)** Data are pooled from 2–3 independent experiments, n=5–9 per group. Error bars are mean ± standard deviation. All statistical tests were two-sided. ns, not significant (p>0.05); *p<0.05; **p<0.01; ***p<0.001; ****p<0.0001. Statistical significance was determined by one-way ANOVA with Tukey's post-test **(d–f, j)** or unpaired t-test **(g–h)**.

P2RX7 preserves T_{PEX} and TR_{TEX} diversity while limiting terminal dysfunction

Having established that P2RX7 preserves T_{PEX} and TR_{TEX} cell abundance, we next asked whether it also maintains the quality and diversity of these pools. P2RX7-KO T_{PEX} and TR_{TEX} cells showed reduced IFN-γ production, diminished effector- and residency-associated markers, and increased terminal exhaustion-associated proteins such as CTLA-4 (**Fig. 2a–c**, **Extended Data Fig. 3a,b**). High-dimensional InfinityFlow profiling further showed that P2RX7-KO cells were restricted across exhausted $CD8^+$ T cell states, with reduced representation of T_{PEX}-like phenotypes and enrichment of terminal dysfunction markers including CD38 and CD39, even within T_{PEX} (**Fig. 2d–f**, **Extended Data Fig. 3c,d**, **Supplementary Table 2**).

Consistent with these phenotypic changes, scRNA-seq revealed that P2RX7 loss narrowed transcriptional diversity within T_{PEX} and TR_{TEX} compartments (**Extended Data Fig. 4a**). Reclustering identified multiple T_{PEX} states, all of which were reduced in P2RX7-KO cells (**Fig. 2g–i**, **Extended Data Fig. 4b-d**). TR_{TEX} reclustering similarly revealed loss of memory-like resident states in P2RX7-KO cells (**Extended Data Fig. 4e-g**). Thus, P2RX7 maintains the functional and transcriptional breadth of progenitor and resident exhausted $CD8^+$ T cells while limiting collapse toward terminal dysfunction.

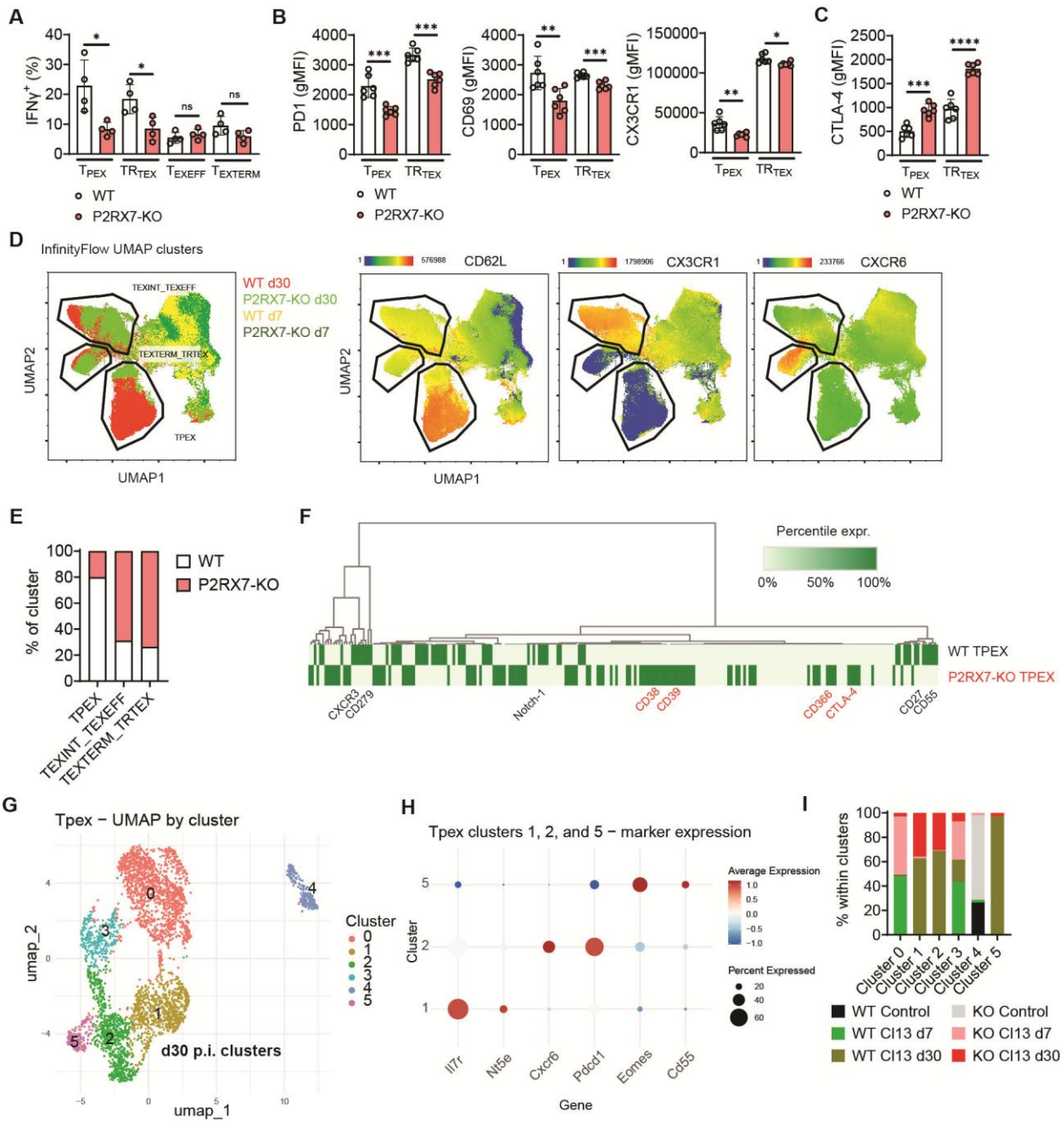


Fig. 2. P2RX7 preserves functional and transcriptional diversity of exhausted CD8⁺ T cells. (a–c) WT and P2RX7-KO P14 cells were analyzed at day 30 p.i. for cytokine production and surface-marker expression. **(d–f)** LEGENDScreen/InfinityFlow profiling of WT and P2RX7-KO P14 cells isolated at days 7 and 30 p.i.; UMAPs, cluster frequencies, differential marker expression, and Wanderlust trajectory analysis are shown. **(g–i)** scRNA-seq analysis of WT and P2RX7-KO P14 cells isolated at days 0, 7, and 30 p.i.; reclustered T_{PEX} states, marker expression, and WT/P2RX7-KO proportions are shown. **(a–c)** Data are pooled from 2 independent experiments, n=4–6 per group. Error bars are mean ± standard deviation. All statistical tests were two-sided. ns, not significant (p>0.05); *p<0.05; **p<0.01; ***p<0.001; ****p<0.0001. Statistical significance was determined by one-way ANOVA with Tukey's post-test.

P2RX7 maintains early exhausted progenitor competence

Because defects in mature T_{PEX} and TR_{TEX} pools could arise during early fate specification, we next asked whether P2RX7 acts at the progenitor stage of exhaustion. Early

T_{PEX} cells emerging during chronic infection expressed high P2RX7 (**Fig. 3a**, **Extended Data Fig. 5a**), and P2RX7 loss reduced their frequency and skewed them toward terminal exhaustion-associated phenotypes as depicted from InfinityFlow analyses (**Fig. 3b,c**, **Extended Data Fig. 5b,c**).

To test whether these early defects altered later developmental potential, we transferred sorted WT or P2RX7-KO early T_{PEX} cells into infection-matched hosts (**Fig. 3d**). P2RX7-KO early T_{PEX} cells expanded poorly and generated fewer T_{PEX} and TR_{TEX} progeny than WT cells (**Fig. 3e–g**). Among WT early T_{PEX} cells, the P2RX7^{hi} fraction produced more daughter cells than the P2RX7^{lo} fraction, and P2RX7 expression within progeny correlated with retention of T_{PEX} and TR_{TEX} fates (**Extended Data Fig. 5d-f**). These findings place P2RX7 at an early, dynamic checkpoint that preserves progenitor competence and enables later expansion into durable T_{PEX} and TR_{TEX} lineages.

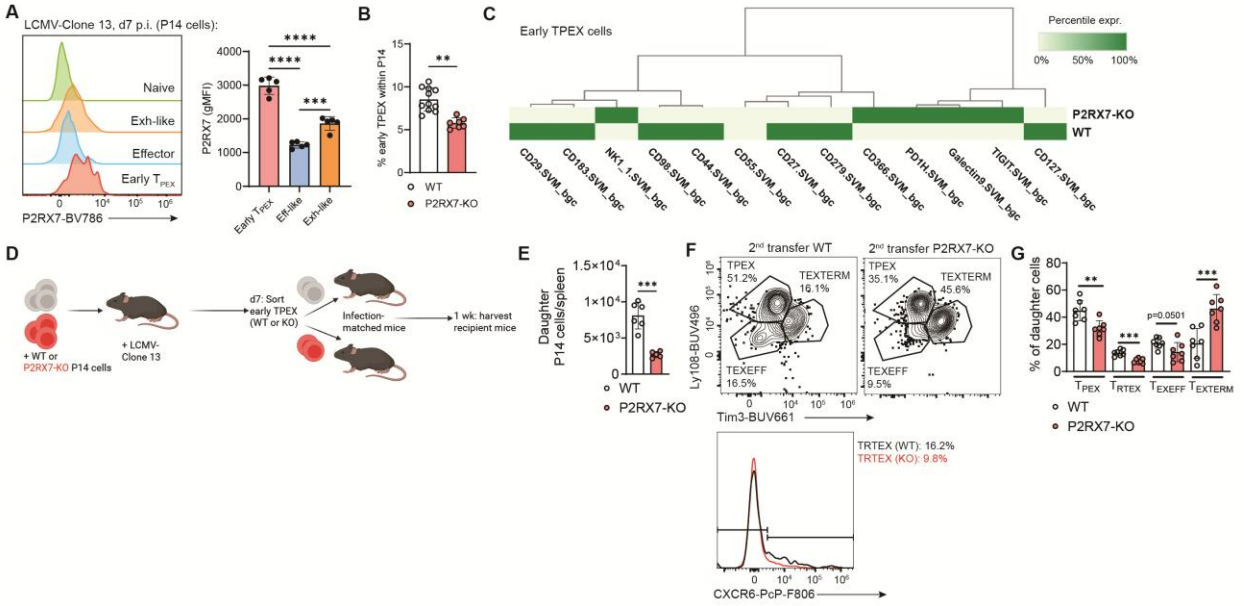


Fig. 3. P2RX7 preserves early exhausted progenitor competence. (a–c) P2RX7 expression, early T_{PEX} frequency, and differential marker expression in WT and P2RX7-KO P14 cells at day 7 p.i. **(d–g)** Sorted WT or P2RX7-KO early T_{PEX} cells were transferred into infection-matched hosts; daughter-cell numbers and exhausted subset frequencies were measured one week later. **(a–b, e–g)** Data are pooled from 2–3 independent experiments, n=5–11 per group. Error bars are mean ± standard deviation. All statistical tests were two-sided. ns, not significant (p>0.05); **p<0.01; ***p<0.001; ****p<0.0001. Statistical significance was determined by one-way ANOVA with Tukey's post-test **(a, g)** or unpaired t-test **(e)**.

P2RX7 sustains mitochondrial fitness and limits lipid oxidative stress

Because durable exhausted progenitor and resident states require metabolic resilience, we next asked whether P2RX7 protects mitochondrial fitness under chronic stimulation. P2RX7-KO T_{PEX} cells showed enrichment of metabolic dysregulation pathways, reduced oxygen consumption, increased glycolytic bias, and diminished protein synthesis despite elevated ECAR (**Fig. 4a–c**). SCENITH and mitochondrial dye analyses further showed reduced mitochondrial support for protein synthesis, lower membrane potential and mitochondrial mass, and impaired fatty acid oxidation-associated protein synthesis capacity in P2RX7-KO T_{PEX} and TR_{TEX} cells (**Fig. 4d–f**, **Extended Data Fig. 6a–c**). These data indicate that P2RX7 sustains mitochondrial fitness and oxidative metabolic capacity in T_{PEX} and TR_{TEX} cells.

This metabolic defect was accompanied by terminal skewing and lipid oxidative stress. P2RX7-KO T_{PEX} cells expressed higher BLIMP-1, and *Prdm1* knockdown partially rescued their *in vivo* deficit (**Fig. 4g,h**, **Extended Data Fig. 6d**). P2RX7-KO T_{PEX} and TR_{TEX} cells also showed increased cell death and lipid peroxidation (**Fig. 4i**, **Extended Data Fig. 6e**). Together, these findings show that P2RX7 protects exhausted $CD8^+$ T cells from a coordinated metabolic failure program marked by mitochondrial dysfunction, BLIMP-1-associated terminal skewing, and lipid peroxidation-associated stress.

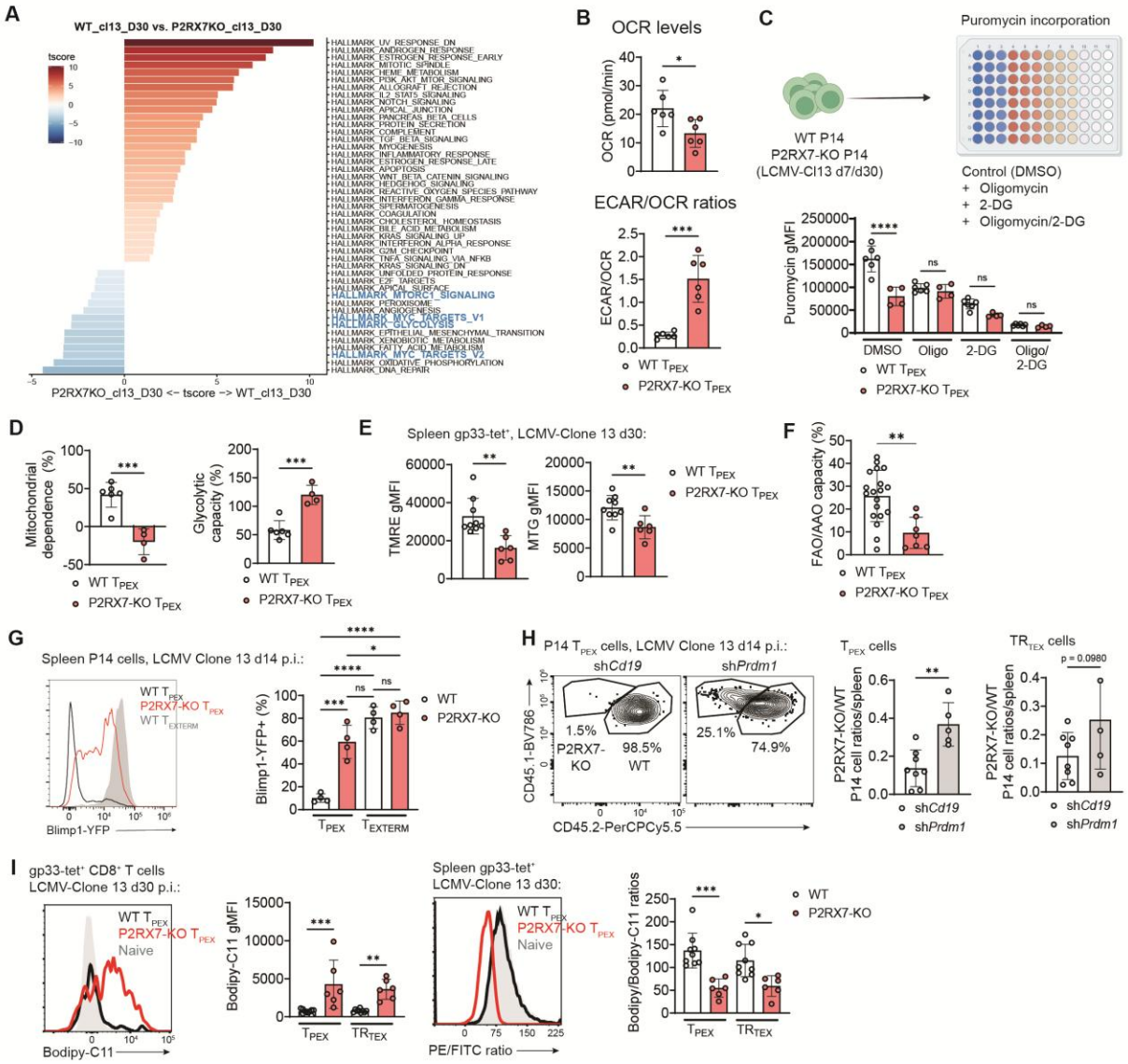


Fig. 4. P2RX7 preserves mitochondrial fitness and limits lipid peroxidation in exhausted $CD8^+$ T cells. (a) Hallmark pathway analysis of WT and P2RX7-KO P14 cells at day 30 p.i. after LCMV-Clone 13 infection; adjusted p value cutoff, <0.05. **(b)** Seahorse analysis of sorted WT and P2RX7-KO T_{PEX} cells showing OCR and ECAR/OCR ratios. **(c and d)** SCENITH analysis of WT and P2RX7-KO P14 cells showing puromycin incorporation, mitochondrial dependence, and glycolytic capacity. **(e and f)** TMRE, MitoTracker Green, and FAO/AAO analysis in WT and P2RX7-KO T_{PEX} cells. **(g)** BLIMP-1 expression in WT and P2RX7-KO T_{PEX} and T_{EXTERM} P14 subsets at day 14 p.i. **(h)** WT and P2RX7-KO P14 cells transduced with control sh*Cd19* or sh*Prdm1* vectors were analyzed for P2RX7-KO/WT ratios among T_{PEX}- and TR_{TEX}-phenotype cells at day 7 p.i. **(i)** BODIPY and BODIPY-C11 staining were used to assess total and oxidized lipid signals in WT and P2RX7-KO T_{PEX} and TR_{TEX} cells at day 30 p.i. **(b–i)** Data are pooled from 2–3 independent experiments, n=4–18 per group. Error bars are mean ± standard deviation. All statistical tests were two-sided. ns, not significant (p>0.05); *p<0.05; **p<0.01; ***p<0.001; ****p<0.0001. Statistical significance was determined by one-way ANOVA with Tukey's post-test **(c, g, i)** or unpaired t-test **(b, d–f, h)**.

P2RX7-dependent Ca^{2+} signaling sustains NFAT/AP-1 activity

We next sought to connect extracellular ATP sensing to the metabolic and fate effects of P2RX7. The P2RX7 inhibitor A-438079 reduced Ca^{2+} uptake in *ex vivo* T_{PEX} and TR_{TEX} cells, and ionomycin restored cell recovery and T_{PEX}-like phenotypes in P2RX7-KO chronically stimulated $CD8^+$ T cells (**Fig. 5a–e**). These results identify P2RX7-dependent Ca^{2+} influx as a proximal signal that sustains exhausted progenitor-like $CD8^+$ T cell states.

We then asked whether this Ca^{2+} signal converges on transcriptional programs that shape exhausted T cell fate. P2RX7-KO exhaustion-like $CD8^+$ T cells showed reduced expression of AP-1 factors, especially JunB (**Fig. 5f,g**, **Extended Data Fig. 7a,b**). Enforced NFAT activation or JunB overexpression increased recovery of P2RX7-KO exhausted $CD8^+$ T cells and restored mitochondrial membrane potential, with JunB rescuing T_{PEX} and TR_{TEX} populations *in vivo* (**Fig. 5h–j**, **Extended Data Fig. 7c**). These data connect P2RX7-dependent Ca^{2+} signaling to NFAT/AP-1 activity upstream of mitochondrial fitness and T_{PEX}/TR_{TEX} preservation.

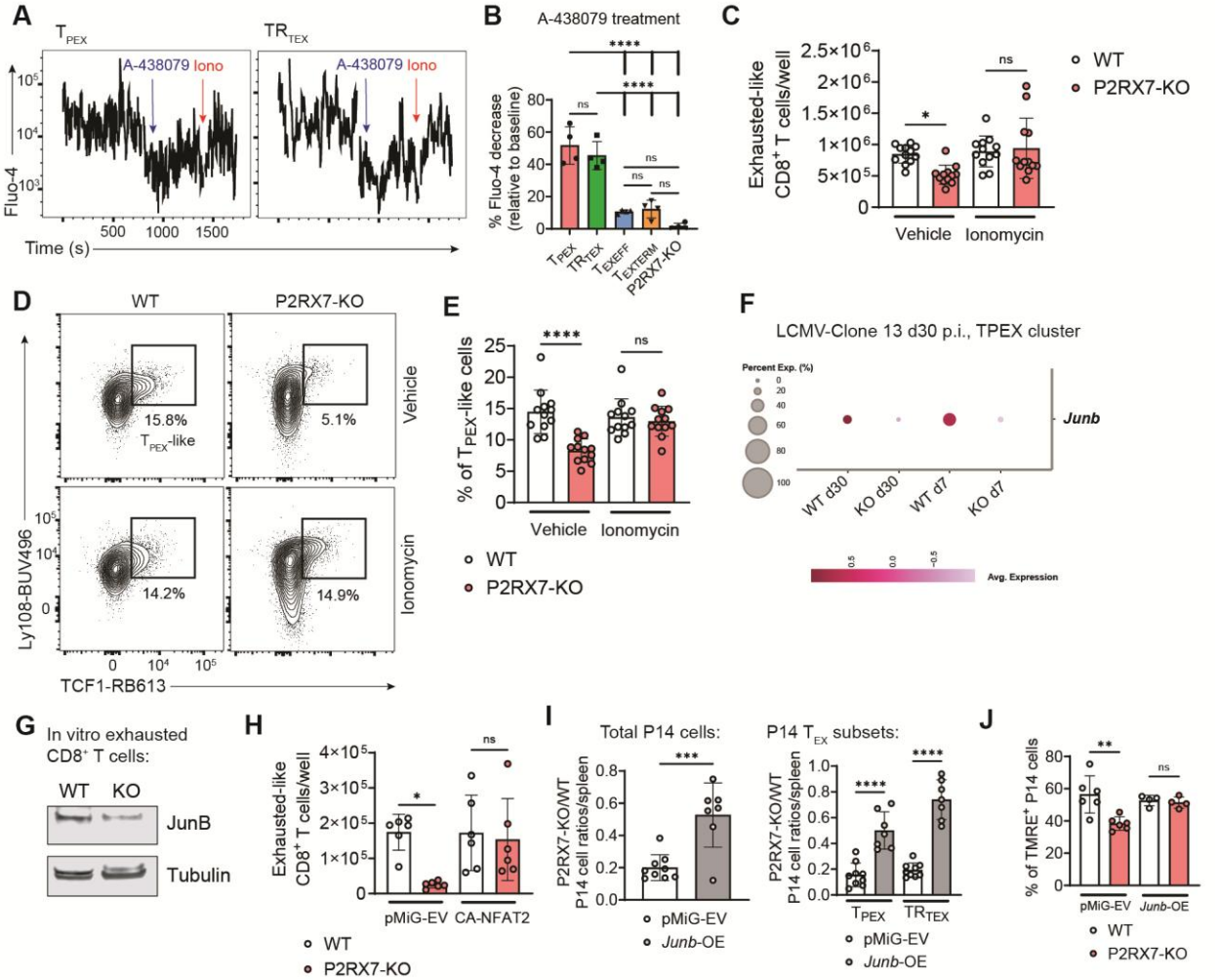


Fig. 5. P2RX7-dependent Ca^{2+} signaling sustains NFAT/AP-1 activity and mitochondrial fitness. (a and b) Fluo-4 calcium-flux analysis of T_{PEX} and TR_{TEX} P14 cells from LCMV-Clone 13-infected mice at day 30 p.i. after A-438079 and ionomycin treatment. **(c–e)** WT and P2RX7-KO $CD8^+$ T cells were chronically activated *in vitro* and treated with vehicle or ionomycin during the final 24 h; cell recovery and T_{PEX}-like frequencies are shown. **(f and g)** *Junb* expression and JunB protein levels in WT and P2RX7-KO exhausted $CD8^+$ T cells. **(h–j)** Effects of constitutively active NFAT2 or *Junb* overexpression on P2RX7-KO exhausted $CD8^+$ T cell recovery, T_{PEX}/TR_{TEX} representation, and TMRE signal. **(b–c, e, h–j)** Data are pooled from 2–3 independent experiments, n=4–12 per group.

Error bars are mean ± standard deviation. All statistical tests were two-sided. ns, not significant (p>0.05); *p<0.05; ****p<0.0001. Statistical significance was determined by one-way ANOVA with Tukey's post-test **(b–c, e, h, j)** or unpaired t-test **(i)**.

KLF3 restores mitochondrial fitness and exhausted subset development downstream of P2RX7

To identify the transcriptional effector linking P2RX7-dependent signaling to metabolic resilience and exhausted subset maintenance, we focused on KLF3. Among the most reduced genes in P2RX7-KO T_{PEX} and TR_{TEX} cells, we identified *Klf3* (**Fig. 6a**), and KLF3 protein was similarly reduced in P2RX7-KO exhaustion-like $CD8^+$ T cells (**Fig. 6b**). KLF3 has been linked to T cell homing and residency programs[27,28] and to fatty acid oxidation and mitochondrial health in other cell types[29,30]. To test whether KLF3 functions downstream of P2RX7, we used tamoxifen-inducible *Klf3* overexpression. KLF3 restoration increased tissue-homing markers and reduced circulating markers in T_{PEX} and TR_{TEX} cells (**Fig. 6c**, **Extended Data Fig. 8**), restored mitochondrial membrane potential and mass (**Fig. 6d**), rescued T_{PEX} and TR_{TEX} numbers *in vivo* (**Fig. 6e**), and partially normalized BLIMP-1 expression in P2RX7-KO T_{PEX} cells (**Fig. 6f**). *Klf3* mRNA expression is partially rescued in P2RX7-KO exhausted $CD8^+$ T cells by enforced NFAT2 activation or JunB overexpression (**Fig. 6g**), suggesting P2RX7-mediated Ca^{2+} pathways at least partially drive KLF3 in exhausted $CD8^+$ T cells. Thus, KLF3 links P2RX7-dependent signaling to residency-associated differentiation, mitochondrial resilience, and exhausted $CD8^+$ T cell subset maintenance (**Fig. 6h**).

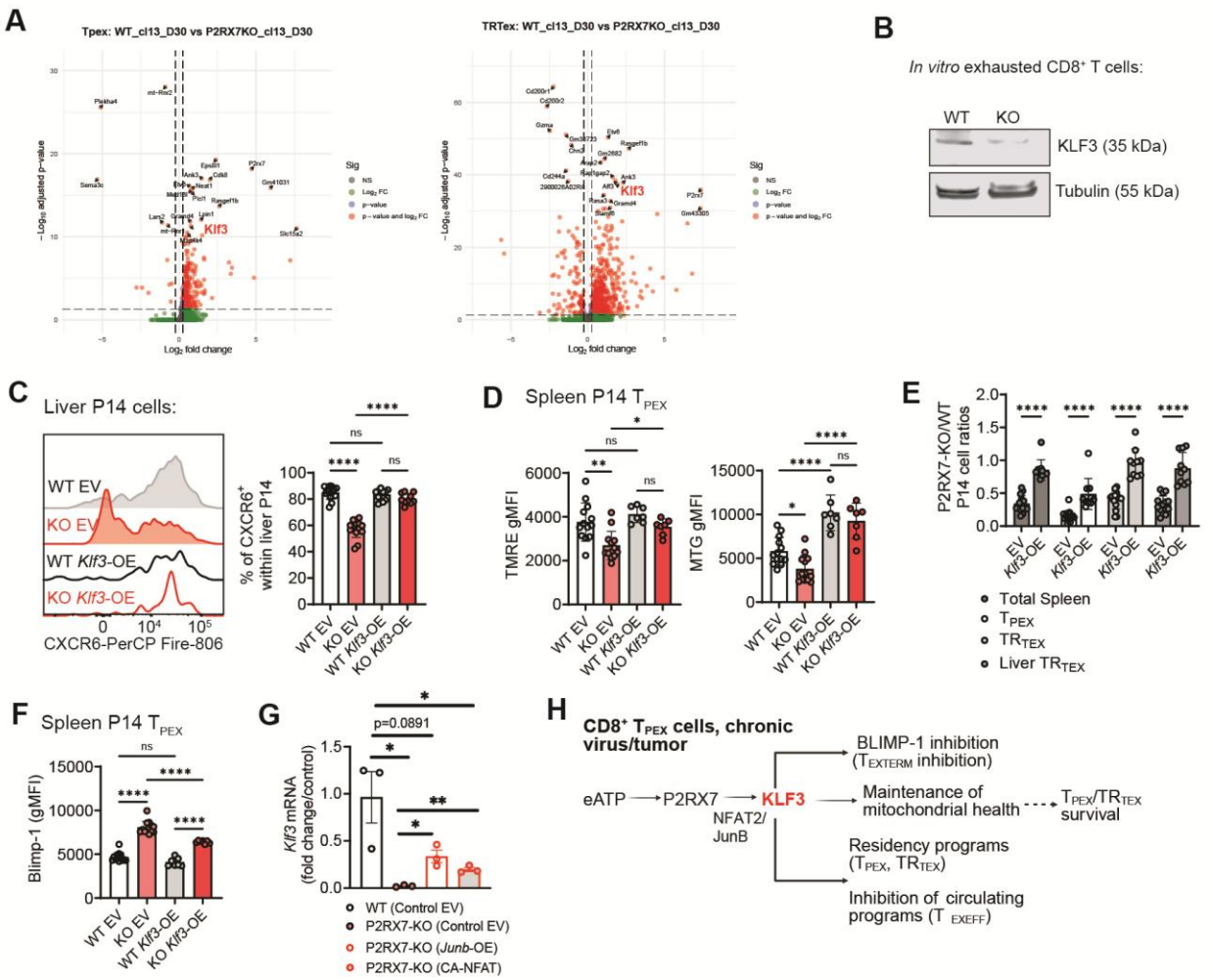


Fig. 6. KLF3 restores mitochondrial and residency-associated programs downstream of P2RX7. (a) Z-score-normalized *Klf3* expression in WT and P2RX7-KO P14 T_{PEX} and TR_{TEX} clusters from day 30 p.i. scRNA-seq analysis after LCMV-Clone 13 infection. **(b)** Western blots showing KLF3 expression in WT and P2RX7-KO splenic and liver P14 cells at day 7 p.i. **(c–f)** WT and P2RX7-KO P14 cells were transduced with empty vector (EV) or tamoxifen-inducible *Klf3*-overexpression (OE) vectors. A 1:1 mixture of EV- or *Klf3*-OE-transduced WT and P2RX7-KO P14 cells was transferred into LCMV-Clone 13-infected recipients, and tamoxifen was administered from days 1 to 5 p.i. CXCR6 expression in liver P14 cells, TMRE and MTG gMFI, P2RX7-KO/WT ratios among total splenic cells, splenic T_{PEX}, splenic TR_{TEX}, and liver TR_{TEX} cells, and BLIMP-1 gMFI in T_{PEX} cells are shown. **(g)** *Klf3* mRNA levels in the indicated WT and P2RX7-KO *in vitro* exhausted $CD8^+$ T cells are shown**. (h)** Model summarizing how P2RX7-dependent extracellular ATP sensing may induce KLF3 through NFAT/JunB-associated signaling to support mitochondrial fitness, residency-associated marker expression, and T_{PEX}/TR_{TEX} maintenance. **(c–g)** Data are pooled from 2 independent experiments, n=3–10 per group. Error bars are mean ± standard deviation. All statistical tests were two-sided. ns, not significant (p>0.05); *p<0.05; **p<0.01; ***p<0.001; ****p<0.0001. Statistical significance was determined by one-way ANOVA with Tukey's post-test.

KLF2 repression enables P2RX7 expression in progenitor and resident exhausted states

Having defined P2RX7-dependent KLF3 activity as a downstream effector program, we next asked how P2RX7 expression is licensed in progenitor and resident exhausted states. Although P2RX7 protein was selectively enriched in T_{PEX} and TR_{TEX} cells, ATAC-seq showed that the *P2rx7* locus remained accessible across exhausted $CD8^+$ T cell states (**Fig. 7a**). Histone profiling revealed activation-associated H3K4me3 and H3K27Ac marks at the *P2rx7* locus in T_{PEX} cells and repressive H3K27me3 marks in terminally exhausted subsets (**Fig. 7a**). CUT&TAG identified KLF2 occupancy at the *P2rx7* promoter and enhancers (**Fig. 7a**). KLF2, a

regulator of tissue egress[28,31,32], and P2RX7 protein expression were inversely correlated in T_{PEX} and TR_{TEX} cells (**Fig. 7b**). To test this relationship functionally while avoiding survival defects associated with KLF2 deletion in exhausted $CD8^+$ T cells[9], we manipulated KLF2 by retroviral overexpression or knockdown. KLF2 overexpression reduced P2RX7 protein, whereas KLF2 knockdown increased P2RX7 protein, specifically in T_{PEX} and TR_{TEX} cells (**Fig. 7c**). These results identify KLF2 repression as an upstream licensing event that enables P2RX7 expression and entry into the P2RX7-KLF3 program in progenitor and resident exhausted $CD8^+$ T cells.

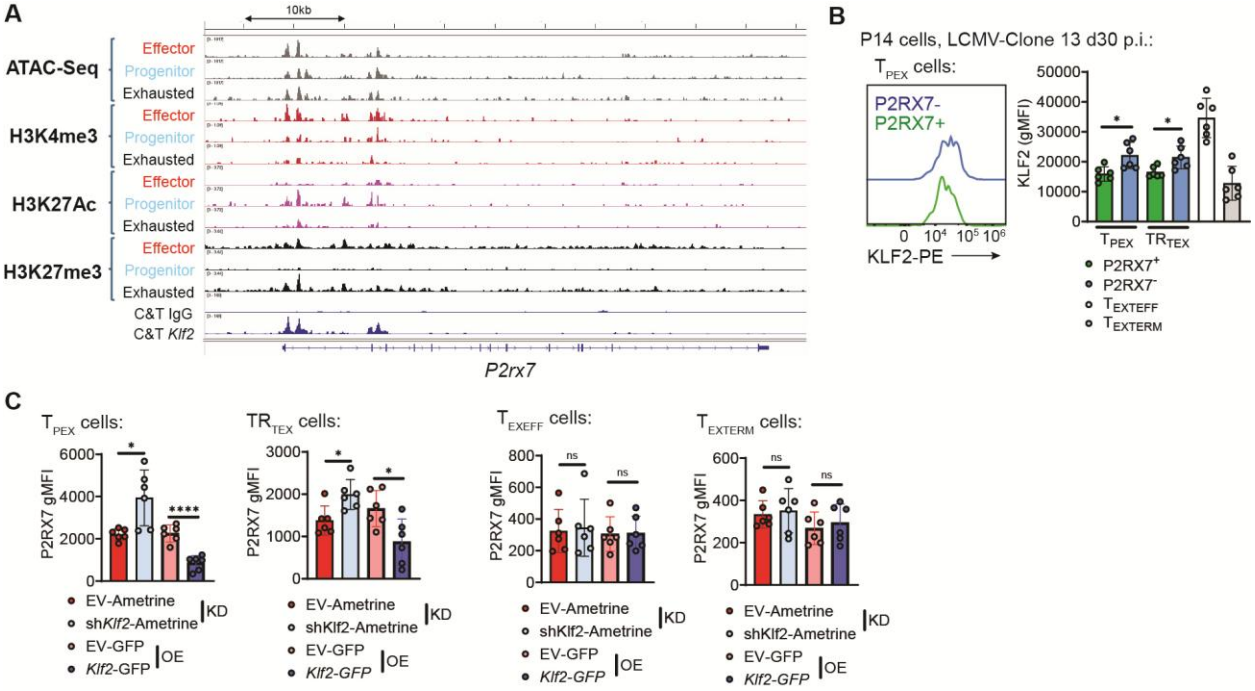


Fig. 7. KLF2 inversely regulates P2RX7 expression in exhausted $CD8^+$ T cell subsets. (a) ATAC-seq and CUT&TAG tracks for H3K4me3, H3K27Ac, H3K27me3, and KLF2 occupancy at the *P2rx7* locus in effector exhausted (T_{EXEFF}), progenitor exhausted (T_{PEX}), and terminally exhausted (T_{EXTERM}) P14 cells from LCMV-Clone 13-infected mice at day 30 p.i. **(b)** KLF2 protein expression in $P2RX7^+$ and $P2RX7^-$ T_{PEX} and TR_{TEX} cells, T_{EXEFF} cells, and T_{EXTERM} cells, shown as representative histograms and gMFI. **(c)** WT P14 cells were transduced with empty vector controls, sh*Klf2*-Ametrine for KLF2 knockdown (KD), or *Klf2*-GFP for KLF2 overexpression (OE), then transferred into LCMV-Clone 13-infected recipients. P2RX7 gMFI in T_{PEX}-, TR_{TEX}-, T_{EXEFF}-, and T_{EXTERM}-phenotype cells at day 7 p.i. is shown. **(b–c)** Data are pooled from 2 independent experiments, n=6 per group. Error bars are mean ± standard deviation. All statistical tests were two-sided. ns, not significant (p>0.05); *p<0.05; ****p<0.0001. Statistical significance was determined by one-way ANOVA with Tukey's post-test.

P2RX7 supports $CD8^+$ T cell responses to PD-1 blockade and can be pharmacologically engaged in preclinical tumor models

Finally, we asked whether P2RX7-dependent preservation of T_{PEX} and TR_{TEX} cells was associated with checkpoint-responsive antitumor immunity. High combined expression of *P2RX7*, *KLF3*, and *CD8B* correlated with improved survival across TCGA PanCancer Atlas datasets, and human lung tumor-infiltrating $CD8^+$ T cells showed P2RX7 enrichment in T_{PEX} and TR_{TEX} subsets (**Fig. 8a,b**). In mouse tumor models, $CD8^+$ T cell-intrinsic P2RX7 deficiency caused modest baseline tumor-control defects but consistently reduced tumor-specific T_{PEX} and TR_{TEX} cells, impaired responses to PD-1 blockade, and limited EGFRvIII-reactive CAR-T cell activity (**Fig. 8c–f**, **Extended Data Fig. 9**). These findings indicate that P2RX7 preserves exhausted $CD8^+$ T cell states associated with effective checkpoint-responsive antitumor immunity.

We then tested whether pharmacologic activation of P2RX7 could enhance antitumor $CD8^+$ T cell immunity in preclinical settings, using ectopic MC38.gp33 and R1LWT tumors. The P2RX7 agonist HEI3090 improved tumor control (**Fig. 8g**), increased tumor-reactive $CD8^+$ T cells in draining lymph nodes (**Fig. 8h**), and sustained T_{PEX} and intratumoral TR_{TEX} populations alone or with anti-PD-1 (**Fig. 8i–k**, **Extended Data Fig. 10a–d**). HEI3090 treatment was also associated with increased memory-like $CD8^+$ T cell accumulation (**Fig. 8l**). Related to this, HEI3090 treatment induced durable tumor clearance and protection from secondary tumor challenge in R1LWT tumor-bearing mice (**Extended Data Fig. 10e**). Together, these data provide preclinical evidence that pharmacologic engagement of P2RX7 can preserve checkpoint-responsive exhausted $CD8^+$ T cell pools and enhance durable antitumor immunity.

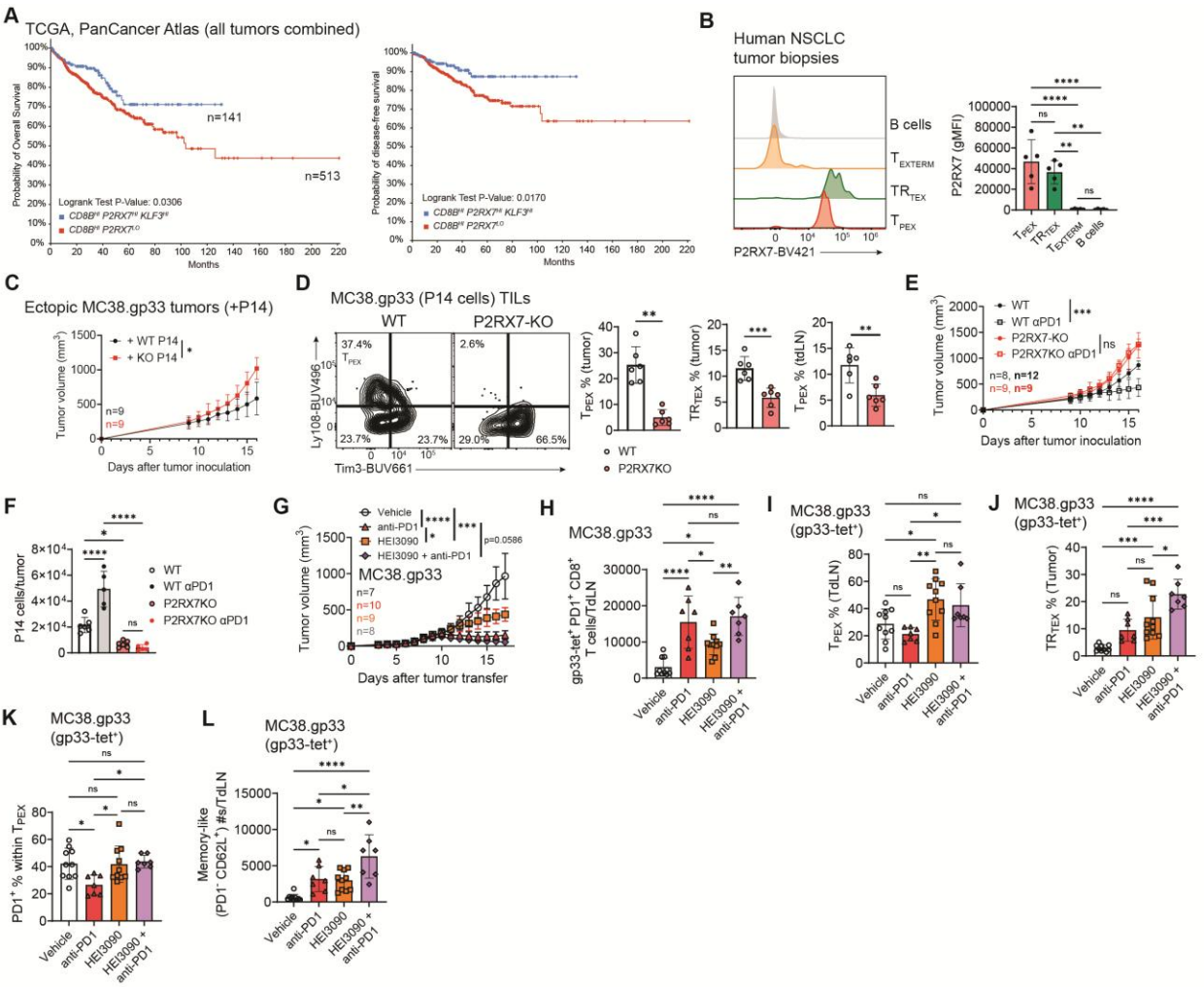


Fig. 8. P2RX7 supports checkpoint-responsive and durable antitumor CD8⁺ T cell immunity. (a) TCGA PanCancer Atlas survival analysis of tumors stratified by combined *CD8B*, *P2RX7*, and *KLF3* expression. **(b)** P2RX7 expression in human NSCLC tumor-infiltrating T_{PEX}, TR_{TEX}, T_{EXTERM}, and B cell populations. **(c–d)** Tumor growth and tumor-specific T_{PEX}/TR_{TEX} responses in MC38.gp33 models with CD8⁺ T cell-intrinsic P2RX7 deficiency (P14 adoptive transfer). **(e-f)** Effects of P2RX7 deficiency or inhibition on anti-PD-1 responses in MC38.gp33 tumor-bearing mice. **(g-k)** MC38.gp33 tumor-bearing WT mice were treated with vehicle, anti-PD-1, HEI3090, or HEI3090 plus anti-PD-1; tumor growth and tumor-reactive T_{PEX}/TR_{TEX} responses are shown. **(l)** Memory-like CD8⁺ T cell accumulation after treatment in MC38.gp33 or R1LWT models. **(b)** Data are from n=5 patients. **(c–l)** Data are pooled from 2–3 independent experiments, n=5–15 per group. Error bars are mean ± standard deviation. All statistical tests were two-sided. ns, not significant (p>0.05); *p<0.05; **p<0.01; ***p<0.001; ****p<0.0001. Statistical significance was determined by one-way ANOVA with Tukey's post-test **(b, f, h-l)**, unpaired t-test **(d)**, or two-way ANOVA with Bonferroni's post-test **(c, e, g)**.

Discussion

Our findings identify extracellular ATP sensing through P2RX7 as a tissue-derived mechanism that supports exhausted CD8⁺ T cell states with therapeutic potential. Exhausted T cells are often defined by transcriptional and epigenetic programs[8–14], but the local cues that preserve progenitor and resident-like subsets during chronic antigen exposure are less well understood. We show that P2RX7 is enriched in T_{PEX} and TR_{TEX} cells and is required cell intrinsically to maintain their persistence, phenotypic diversity and developmental competence. Thus, extracellular ATP, a damage-associated metabolite abundant in inflamed tissues and tumors, can contribute to the maintenance of exhausted CD8⁺ T cell subsets rather than simply reflecting tissue injury.

These data place P2RX7 upstream of a metabolic and transcriptional program that stabilizes exhausted progenitor and resident-like states. P2RX7-dependent Ca^{2+} signaling sustained NFAT/AP-1 activity and was linked to induction of KLF3, a transcription factor associated with tissue residency and metabolic regulation[27–30]. Restoration of KLF3 was sufficient to improve mitochondrial fitness and recover T_{PEX} and TR_{TEX} development in P2RX7-deficient cells. In parallel, repression of KLF2 permitted P2RX7 expression in these populations. Together, these findings suggest that reduced migratory programming[28] enables exhausted $CD8^+$ T cells to sense extracellular ATP, which then reinforces KLF3-dependent metabolic fitness and tissue-adapted persistence.

The metabolic consequences of P2RX7 loss further support a link between tissue sensing and exhausted T cell fate stability. P2RX7-deficient T_{PEX} and TR_{TEX} cells showed impaired mitochondrial respiration, reduced mitochondrial mass and membrane potential, increased BLIMP-1 and elevated lipid peroxidation-associated stress. These defects were accompanied by contraction of progenitor and resident-like compartments and enrichment of terminal exhaustion-associated features. Although P2RX7 has established roles in memory $CD8^+$ T cell fitness and tissue-resident memory differentiation[23–25], our results indicate that, in chronic antigen exposure, the same receptor supports a distinct adaptation: preservation of exhausted $CD8^+$ T cell states under persistent inflammatory and metabolic stress.

These findings have implications for immunotherapy. T_{PEX} cells are a major source of the proliferative response to PD-1 blockade, and tissue-localized exhausted subsets may contribute to immune control within tumors and chronically infected tissues. By preserving both compartments, P2RX7 supported $CD8^+$ T cell responses to PD-1 blockade in preclinical models. Pharmacologic activation of P2RX7 enhanced tumor control and was associated with durable protection in mouse tumor models, raising the possibility that selected microenvironmental sensing pathways could be leveraged to sustain therapeutically responsive exhausted T cells. This idea will require further study, as P2RX7 is expressed by several immune and nonimmune populations and can promote context-dependent inflammation and distinct effects in other immune cells[33]. Future work should define the cellular targets of P2RX7 agonism, the tissue settings in which this pathway is beneficial, and the pharmacologic conditions that separate T cell-supportive activity from inflammatory toxicity. More broadly, our results suggest that chronic tissue damage can provide instructive signals that help preserve, rather than only erode, exhausted $CD8^+$ T cell function.

Methods

Study design

This study investigated how extracellular ATP sensing regulates exhausted $CD8^+$ T cell development and antitumor immunity. For *in vitro* experiments, primary mouse $CD8^+$ T cells were subjected to chronic stimulation through successive cycles of anti-CD3 antibody stimulation. For *in vivo* experiments, mice were infected with LCMV-Clone 13 or LCMV-Armstrong or inoculated with ectopic (MC38.gp33, R1LWT, or B16.EGFRvIII) or orthotopic (EO771-OVA) tumors. Experimental approaches included single-cell RNA-seq, flow cytometry, LEGENDScreen/InfinityFlow, western blotting, co-immunoprecipitation, Seahorse analysis, single-cell ATAC-seq, and CUT&TAG analysis. Male and female mice (6- to 8-weeks old) were randomly allocated to experimental groups with a minimum of three mice per group per

experimental replicate. Tumor area was monitored throughout the study and did not exceed 144 mm^2, in accordance with the predefined humane endpoint. Investigators were not blinded during treatment administration, but all outcome assessments were performed in a blinded manner. All experiments included two or three independent biological replicates, and technical replicates are specified in the corresponding figure legends.

Mice

C57BL/6, CD45.1 (B6.SJL-*Ptprc*^{a} *Pepc*^{b}/BoyJ), CD4-Cre (B6.Cg-Tg(Cd4-cre)1Cwi/BfluJ), CD8-Cre (C57BL/6-Tg(Cd8a-cre)1Itan/J), and Blimp1-YFP (B6.Cg-Tg(Prdm1-EYFP)1Mnz/J) mice were purchased from The Jackson Laboratory and bred in-house. LCMV-D^b gp33-specific TCR transgenic P14 mice were bred in-house at Mayo Clinic Arizona. *P2rx7*$^{fl/fl}$ mice were obtained from Gyorgy Hasko (Rutgers University) and Matyas Sandor (University of Wisconsin) and bred in-house. Mice were maintained in a specific pathogen-free facility at Mayo Clinic Arizona. All experiments were performed in accordance with protocols approved by the Mayo Clinic Arizona Institutional Animal Care and Use Committee (IACUC; protocols A00005172-20-R25 and A00005542-20-R23).

LCMV infections

WT (CD8-Cre, C57BL/6) or CD8-Cre *P2rx7*$^{fl/fl}$ mice were infected with LCMV-Clone 13 ($2x10^6$ PFU, intravenously (i.v.)) or LCMV-Armstrong ($2x10^5$ PFU, intraperitoneally (i.p.)). In some experiments, WT or P2RX7-KO (CD4-Cre *P2rx7*$^{fl/fl}$) P14 cells were adoptively transferred into naïve WT mice, which were infected with LCMV-Clone 13. LCMV titers were measured using quantitative PCR as previously described[34].

Mouse tumor models

For ectopic tumor models, WT or CD8-Cre *P2rx7*$^{fl/fl}$ mice were injected subcutaneously with MC38.gp33 ($2x10^5$), B16.EGFRvIII ($2x10^5$), or R1LWT ($2.5x10^5$) cells in the right flank. In some experiments, MC38-bearing mice were adoptively transferred with WT or P2RX7-KO P14 cells ($5x10^5$ cells/mouse) before tumor inoculation. For CAR-T cell experiments, WT or P2RX7-KO $CD8^+$ T cells were transduced with a retroviral vector encoding the EGFRvIII-CAR construct[35] and then adoptively transferred into mice bearing B16.EGFRvIII tumors. For orthotopic tumor models, WT or CD4-Cre *P2rx7*$^{fl/fl}$ mice were injected directly into the mammary fat pads with EO771-OVA cells ($5x10^4$). In all cases, tumor growth was monitored by measuring height, width, and/or depth with calipers until mice reached endpoint criteria. When indicated in the figures, tumor-bearing mice were euthanized for flow cytometry analysis. In some experiments, MC38.gp33 or R1LWT tumor-bearing mice were treated with anti-PD-1 antibodies (BioXCell; 200 µg/mouse/day) and/or HEI3090 (MedChemExpress; 0.06 g/mouse/day) every other day between days 7 and 14 post-tumor inoculation.

Tissue collection and processing

Lymphocytes were isolated from tissues including spleen, inguinal lymph nodes, cervical lymph nodes, blood, liver, and tumors[23,24,36]. Briefly, organs were removed and cut into small pieces in Erlenmeyer flasks containing 30 mL of 0.5 mg/mL collagenase type I solution for tumors or 0.5 mg/mL collagenase type II solution for livers. Lymphocytes were then isolated by 44/67% Percoll gradient separation. For lymphocyte isolation from non-lymphoid tissues, 50 µg of Treg-

Protector (anti-ARTC2.2) nanobodies (BioLegend) was injected intravenously 30 min before mouse sacrifice in all experiments[37]. Blood leukocytes were isolated by incubation with ACK lysis buffer made in-house, followed by two washes with FACS buffer. Spleens and lymph nodes were processed by mechanical disruption through cell strainers, followed by ACK lysis buffer incubation for spleens and two washes with FACS buffer.

Flow cytometry

Direct *ex vivo* staining and intracellular staining were performed as described[23]. To identify LCMV-specific (MC38.gp33-specific) and OVA-specific $CD8^+$ T cells, tetramers were obtained from the Yerkes NIH Tetramer Core: D^b-gp33 and K^b-SIINFEKL tetramers conjugated with BV421-Streptavidin, Alexa Fluor 680-Streptavidin or PE-Streptavidin were used. To detect tumor-reactive $CD8^+$ T cells from R1LWT tumors or NSCLC biopsies, we used co-expression of CD11a and CD44. The subsets of exhausted/tumor-reactive $CD8^+$ T cells studied from these models can be found in **Extended Data Fig. 1**. Adoptively transferred P14 cells were identified using a combination of CD45.1 and CD45.2 monoclonal antibodies. Retrovirally transduced $CD8^+$ T cells were identified using either anti-Thy1.1 antibodies (pMiG-EV, *Prdm1*-OE, *Klf3*-OE), GFP (*Klf2*-OE, *Junb*-OE, CA-NFAT2, pMiG-GFP) or Ametrine (sh*Klf2*-KD, sh*Cd19*-KD). From *in vitro* cultured exhausted-like $CD8^+$ T cells, we used antibodies for CD44, PD1, Tim-3, Ly108, TCF-1 and TOX. In all flow cytometry experiments, Live/Dead Near-IR was used to distinguish between live and dead cells. Intracellular detection of transcription factors (KLF2, TCF-1, TOX, T-bet) and cytokines (Granzyme B, TNFα and IFNγ) was done as described before[23]. For mitochondrial mass and membrane potential measurements, cells were incubated with Mitotracker Green (Thermo Fisher Scientific) and TMRE (Cell Signaling Technology) simultaneously for 15 min at 37°C prior to staining. In some experiments, *ex vivo* or *in vitro* exhausted $CD8^+$ T cells were incubated with Fluo-4 (1 μM) prior to flow cytometry measurements, which were done as previously described[38]. Bodipy (PE)/Bodipy C:11 (FITC) stainings were done following the manufacturer's instructions (ThermoFisher); the PE/FITC ratio pseudo channel (proxy for normalized lipid peroxidation levels) was generated in FlowJo v11 software, as previously described[39]. Flow cytometric analyses were performed on FACS Symphony (BD Biosciences), or 5-laser Aurora (Cytek) and data was analyzed using FlowJo v11 software (BD Biosciences).

Single-cell RNA-seq experiments

WT and P2RX7-KO P14 cells were isolated from host mice at days 7 or 30 post-infection with LCMV-Clone 13 or LCMV-Armstrong (samples were collected from n=5 mice per experimental group). Single-cell libraries (100,000 cells across all groups) were prepared using the Evercode Whole Transcriptome kit (Parse Biosciences) following the manufacturer's instructions. Briefly, cells were fixed using the Parse Cell Fixation Kit (Parse Biosciences) and immediately barcoded with the Evercode Whole Transcriptome kit. Sequencing was performed at the Collaborative Sequencing Center (Translational Genomics Research Institute, Phoenix, AZ) using the Illumina NovaSeq X Plus 25B platform with 300 cycles. Raw sequencing reads were processed using ParseBio's Trailmaker software (v1.6.0) to generate cell-count matrices. Cell profiles with >20% mitochondrial content were excluded from the analyses. Clustering was performed using Scanpy (v1.11.5)[40]. Gene expression counts were normalized to 10,000 reads per cell, log-transformed, and the top 500 highly variable genes were identified.

Dimensionality reduction was performed using PCA, and the top 50 principal components were used to build a k-nearest-neighbor graph (k = 15), which was then used to generate a UMAP embedding. Clusters were defined using the Leiden algorithm. Cluster annotation was performed using the ProjecTILs R package, by projecting query cells onto a custom CD8 T cell reference atlas annotated by functional T cell states. TR_{TEX}-like cells were further annotated by incorporating a TR_{TEX} signature score based on previously described TR_{TEX} markers[7]. Reclustering within each ProjecTILs-annotated cluster was performed in Seurat by subsetting each functional population and applying graph-based clustering in the RNA PCA space using the first 25 principal components, followed by Leiden clustering across multiple resolutions. Within each reanalyzed cluster, differentially expressed genes (DEGs) were identified using Seurat FindMarkers/FindAllMarkers. Pathway enrichment was assessed using Hallmark gene sets with AUCell-based gene set scoring, followed by differential pathway activity analysis across clusters and experimental groups.

LEGENDScreen and InfinityFlow data analysis

Two datasets were generated in this study: a comparison between WT and P2RX7-KO P14 cells obtained from spleens of mice at days 7 or 30 post-infection with LCMV-Clone 13, and a comparison between WT and P2RX7-KO P14 cells obtained from spleens of mice exclusively at day 7 post-LCMV-Clone 13 infection. For all datasets, $CD8^+$ T cells were enriched using $CD8^+$ T cell enrichment kits (StemCell Technologies). Enriched suspensions from each sample were stained with distinct combinations of biotinylated anti-CD45.1 and/or anti-CD45.2 and were barcoded using distinct streptavidin combinations before pooling (see **Extended Data Fig. 4c**). Cells were then resuspended at $2x10^7$ cells/mL and stained in FACS buffer (PBS + 2% FBS) with anti-CD16/32 (FcBlock) and Live/Dead Near-IR for 30 min at 4°C. After washing, cells were stained with the backbone antibody panel for 60 min at room temperature (see **Extended Data Fig. 4c**). After washing, cells were resuspended at $4x10^6$ cells/mL and aliquoted into each well of the LEGENDScreen Mouse PE Kit (BioLegend), followed by staining for 45 min at 4°C according to the manufacturer's instructions. After washing and fixation with BioLegend fixation buffer, cells were resuspended in 100 µL/well and acquired on a 5-laser Cytek Aurora spectral flow cytometer. Following data acquisition, FCS files were individually analyzed in FlowJo (BD Biosciences) for compensation adjustment and quality control as previously described[41]. Following sample cleaning, new FCS files for each well were generated and used as input for the InfinityFlow prediction pipeline using the *infinityFlow* R package[42]. In summary, each channel from the input data, except FSC-A, SSC-A, Live/Dead, and streptavidin barcodes, was scaled using logicle transformation with parameters estimated from the *infinityFlow* R package. Half of the data from each well was randomly selected for training of the XGBoost nonlinear regression model (*xgboost* R package) with a depth of 500 trees, a learning rate of 0.05, and remaining default parameters. From the non-training data, 30,000 events were randomly selected per well and concatenated to generate the backbone matrix of the InfinityFlow output. Predictions from all models were generated across all non-training events to generate the final InfinityFlow matrix. These predictions were concatenated and dimensionally reduced with UMAP on backbone parameters to generate a single data matrix (>200 dimensions), using the *uwot* R package with parameters n_neighbors = 15, min_dist = 0.2, metric = "euclidean," and n_epochs = 2000. The InfinityFlow-augmented data matrix was scaled using the OMIQ cloud platform as previously described[41]. Additional analyses of the augmented data, such as heatmap comparisons between groups, Wanderlust trajectory inference using default parameters and $CD62L^{hi}$ T_{PEX} as

the starting point, and SPADE analysis for cell clustering, were performed using the OMIQ cloud platform.

Secondary adoptive transfer experiments

For secondary transfer experiments, WT or P2RX7-KO early T_{PEX} ($Ly108^+PD1^+Tim\text{-}3^-$) P14 cells were cell sorted from mice at day 7 post-LCMV Clone 13 infection. Cell sorting was performed on a FACS Aria III device (BD Biosciences). The population purity after cell sorting was > 98% in all experiments.

In vitro exhaustion model

We induced *in vitro* exhaustion as previously described[43]. Polyclonal $CD8^+$ T cells were isolated from spleens of naïve WT or CD8-Cre *P2rx7*$^{fl/fl}$ mice by homogenization through a 70-μm cell strainer. $CD8^+$ T cells were isolated using a $CD8^+$ T cell purification kit (StemCell Technologies), then activated *in vitro* for 48 h with anti-CD3 (10 μg/mL, BioXCell), anti-CD28 (20 μg/mL, BioXCell), and recombinant murine IL-2 (10 ng/mL, Thermo Fisher Scientific). For chronic stimulation, $CD8^+$ T cells were replated every 48 h with anti-CD3 (3 μg/mL) and recombinant murine IL-2 (10 ng/mL); recombinant murine IL-7 and IL-15 (10 ng/mL each; Thermo Fisher Scientific) were added to maintain the viability of chronically cultured $CD8^+$ T cells. Chronically stimulated $CD8^+$ T cells were replated at 48, 96, and 144 h. In some experiments, ionomycin (1 μM) was added to the *in vitro*-exhausted $CD8^+$ T cell wells during the final 24 h of culture.

Western blot

The indicated $CD8^+$ T cell pellets were washed three times in 1x PBS supplemented with 1 mM PMSF. Cells were lysed using 1x RIPA buffer (CST #9806) supplemented with 1 mM PMSF (MilliporeSigma #P7626) and protease/phosphatase inhibitor (Thermo Fisher Scientific #78440). Lysates were incubated on ice for 5 min and sonicated with a 125-W Qsonica sonicator (20% amplitude, 10 s on/10 s off for 1 min; 30 s total sonication). Lysates were kept on ice during off cycles and centrifuged for 10 min at 10,000g; supernatants were retained and pellets were discarded. Lysate concentration was determined using the Pierce BCA Protein Assay Kit (Thermo Fisher Scientific #23225). For loading, 30 μg of protein was mixed with NuPAGE LDS Sample Buffer (Thermo Fisher Scientific #NP0007) and reducing agent (Thermo Fisher Scientific #NP0009). Prepared lysates were boiled at 95°C for 5-10 min and loaded onto a 4-12% NuPAGE Novex Bis-Tris Protein Gel (Thermo Fisher Scientific #NP0321BOX). Gels were run for 45-60 min at 165 V, 800 mA, and 200 W, then transferred to nitrocellulose membranes using the Bio-Rad Trans-Blot Turbo Transfer System according to the manufacturer's recommendations. Membranes were blocked with Odyssey TBS Blocking Buffer (LI-COR #927-60010) for 2 h at room temperature. Primary antibodies were incubated overnight at 4°C in Odyssey TBS Blocking Buffer supplemented with 0.1% Tween-20 at 1:1000 dilution: c-FOS (CST #2250), FosB (CST #2251), c-Jun (CST #9165), JunB (CST #3753), KLF3 (Thermo Fisher Scientific #PA5-95076), and Tubulin (MilliporeSigma #05-829). The next day, membranes were washed three times for 5 min with TBST. Secondary antibodies were diluted 1:15,000 in Odyssey TBS Blocking Buffer supplemented with 0.1% Tween-20 (LI-COR #926-32211 and #926-68050) and incubated for 2 h at room temperature. Membranes were washed three times for 5 min with TBST and imaged on an Odyssey CLx.

RNA extraction and Quantitative Real-Time PCR

RNA was extracted from *in vitro* exhausted $CD8^+$ T cells using the RNAeasy kit (QIAgen). After RNA quantification using Nanodrop, quantitative real-time PCR reactions were done for *Klf3* (forward primer: CCTCTCATGGTTTCCTTGTCGG, reverse primer: CCTCTGTGGTTCAATTCCAGGC), using *Actb* as a housekeeping control. Relative quantification of *Klf3* mRNA was done using the 2(-delta/delta CT) method.

Retroviral transduction experiments

Control empty retroviral vectors (pMiG-EV, EV-GFP, EV-Ametrine, and knockdown of *Cd19* – sh*Cd19*) and vectors for overexpression of *Junb* (pMiG-*Junb*), overexpression of *Klf2* (*Klf2*-GFP), overexpression of *Klf3* (*Klf3*-OE), knockdown of *Klf2* (sh*Klf2*-Ametrine), knockdown of *Prdm1* (sh*Prdm1*) and overexpression of a constitutively active NFAT2 (CA-NFAT2), were produced as retroviral supernatants from HEK293T cells transfected with the corresponding plasmids. HEK293T cells were transfected using PEI 25K (Fisher Scientific) at a 1:3 plasmid-to-PEI ratio and cultured in DMEM supplemented with 10% FBS, 1% penicillin-streptomycin, and 1% sodium pyruvate. *In vitro*-activated P14 cells (after 24 hours of activation) were transduced via spin infection with retroviral supernatants, as previously described[24]. Cells were rested in the presence of IL-2 for 48 additional hours, prior to further experiments.

Extracellular flux analyses

In the indicated ex vivo-sorted $CD8^+$ T cell populations, OCR and ECAR values were measured using a 96-well XF Extracellular flux analyzer, following manufacturer instructions (Agilent)[23]. A total of $1.5x10^5$ $CD8^+$ T cells per well were plated, and wells were pre-treated with CellTak (22.4 μg/mL) prior to cell seeding for better adherence.

SCENITH analyses

SCENITH analyses were performed as previously described[44]. Briefly, cells were seeded in 48-well plates ($1x10^6$ cells/mL) in triplicate per experimental group. Wells were treated for 30-45 min with control (DMSO), 2-deoxy-D-glucose (2-DG, 100 mM), oligomycin (1 μM), or 2-DG plus oligomycin. Puromycin (10 μg/mL) was added to the wells during the final 15 min of treatment. Cells were then washed in cold PBS and stained with Fc block, followed by washing and surface-marker staining for 30 min at room temperature. After washing, cells were fixed and permeabilized with FOXP3 fixation/permeabilization buffer (Thermo Fisher Scientific) according to the manufacturer's instructions. Intracellular staining with anti-puromycin antibody (Alexa Fluor 647) was performed for 1 h at 4°C in permeabilization buffer. Samples were acquired on a 5-laser Cytek Aurora flow cytometer. Glycolytic capacity, mitochondrial dependence, and FAO/AAO were calculated as previously described[44].

Epigenetic analyses of exhausted $CD8^+$ T cells

scMultiome-seq and CUT&TAG datasets (GEO accession numbers GSE222346 and GSE296612) were analyzed as previously described[28].

Human dataset analyses

Survival data from NSCLC patients (patients split by median; n=654) were analyzed using the Kaplan-Meier Plotter tool. Overall survival was evaluated based on *P2RX7*, *CD8B*, and *KLF3*

mRNA expression levels. Patients were stratified into "high" and "low" expression groups according to median *P2RX7*, *CD8B*, and *KLF3* expression values. Kaplan-Meier survival curves were generated, and statistical significance was determined using the log-rank test.

Processing and analyses of human tumor biopsies

Samples (n=5) were collected from patients with non-small cell lung cancer (NSCLC) during biopsy at Mayo Clinic Hospital, Jacksonville. Samples were collected between September and October 2025 from patients with adenocarcinoma of different stages, rapidly frozen, and sent for analysis. Upon arrival, tissues were processed in RPMI medium (Gibco) with 0.5 mg/mL collagenase type IV (Gibco) and subjected to cell separation using GentleMACS. Cells were washed with FACS buffer (PBS 2% FBS) and stained with the following surface antibodies diluted in FACS buffer: anti-human CD4 (Spark UV 395, clone SK3, BioLegend), anti-human CD8 (PerCP, clone SK1, BioLegend, #344701), anti-human CD3 (APC/Fire 810, clone SK7, BioLegend, #344858), anti-human CD19 (BUV563, clone SJ25C1, BD Biosciences, #612917), anti-mouse/human CD44 (BV786, clone IM7, BioLegend, Cat# 103041), anti-mouse P2RX7 (BV421, clone 1F11, BD Biosciences, Cat# 744779; laboratory-optimized staining), anti-human Ly108 (PE, clone W19035D, BD Biosciences, #332304), anti-human Tim-3 (BB515, clone 7D3, BD Biosciences, #565569), and Live/Dead viability dye (Ghost Dye 778). Surface staining was performed for 40 min at room temperature. After staining, cells were washed with FACS buffer and fixed and permeabilized using the True-Nuclear Transcription Factor Buffer Set (BioLegend, Cat# 424401) for 30 min at room temperature. Cells were then washed with kit buffer (PermWash) and stained with anti-human FOXP3 (BB515, clone 236A/E7, eBioscience, #53-4777-42) and anti-human TCF1 (Alexa Fluor 647, clone 7F11A10, BioLegend, #655203) diluted in PermWash overnight at 4°C. Data were acquired on a Cytek Aurora flow cytometer. For P2RX7 identification, fluorescence-minus-one (FMO) control samples were used. Samples were collected after written informed consent was obtained from the patients, and the studies were conducted in accordance with the Declaration of Helsinki. These studies were approved under IRB protocol 14-004094 (Mayo Clinic Florida).

Details on statistical tests are provided in the figure legends. Data were subjected to the Kolmogorov-Smirnov test to assess dataset normality. Statistical differences were calculated using unpaired two-tailed Student's t-test, one-way ANOVA with Tukey's post-test, two-way ANOVA with Bonferroni's post-test, or Kaplan-Meier survival curve analysis, as appropriate. All experiments were analyzed using Prism 10 (GraphPad Software). Graphical data are shown as mean values with error bars indicating the SD. P values of <0.05 (*), <0.01 (**), <0.001 (***), or <0.0001 (****) indicated significant differences between groups.

Acknowledgments: We thank the Laboratory of Immunity to Danger Signals (LIDS) for their intellectual support. We also thank the Flow Cytometry Core at Mayo Clinic Arizona, the Collaborative Sequencing Center at Translational Genomics Research Institute, and the Animal Facility and Flow Cytometry Core staff at Mayo Clinic Arizona for their experimental and logistics support.

Funding:

National Institutes of Health grant R01AI170649 (HBdS)
National Institutes of Health grant P50CA116201 (HBdS)
National Institutes of Health grant P50CA210964 (HBdS)
National Institutes of Health grant R01AI177864 (JJM)

Sao Paulo Research Foundation (FAPESP) 2025/04936-8 (GASS)

Author contributions:

Conceptualization: CLS, HBdS

Methodology: RV, JJM, WC, HBdS

Formal analysis: CLS, HBdS

Investigation: CLS, LK, GASS, ISC, HW, CP, BGM, CY, JS, KG, OL, AB, DKG

Resources: NLT, RV, BH, JAC, JJM, SCJ, WC, HBdS

Visualization: CLS, CY, KG, AB, HBdS

Funding acquisition: NLT, RV, BH, JAC, JJM, SCJ, WC, HBdS

Project administration: HBdS

Supervision: NLT, RV, BH, JAC, JJM, SCJ, WC, HBdS

Writing – original draft: CLS, HBdS

Writing – review & editing: CLS, LK, GASS, ISC, HW, CP, BGM, CY, JS, KG, OL, AB, NLT, RV, BH, JAC, JJM, SCJ, WC, HBdS

Competing interests: BH is a consultant to Intuitive Surgical. All other authors declare that they have no competing interests.

Data and materials availability: Single-cell RNA-seq data are available in the GEO Database under accession number GSE337539. Single-cell multiome-seq data and CUT&TAG data are available in the GEO Database under accession numbers GSE222346 and GSE296612. All data and accession codes are available in the main text or the supplementary materials.

References

1. L. Rausch, A. Kallies, Molecular Mechanisms Governing CD8 T Cell Differentiation and Checkpoint Inhibitor Response in Cancer. *Annu Rev Immunol* **43**, 515-543 (2025).
2. D. Zehn, R. Thimme, E. Lugli, G. P. de Almeida, A. Oxenius, 'Stem-like' precursors are the fount to sustain persistent CD8(+) T cell responses. *Nat Immunol* **23**, 836-847 (2022).
3. L. M. McLane, M. S. Abdel-Hakeem, E. J. Wherry, CD8 T Cell Exhaustion During Chronic Viral Infection and Cancer. *Annu Rev Immunol* **37**, 457-495 (2019).
4. C. U. Blank, W. N. Haining, W. Held, P. G. Hogan, A. Kallies, E. Lugli, R. C. Lynn, M. Philip, A. Rao, N. P. Restifo, A. Schietinger, T. N. Schumacher, P. L. Schwartzberg, A. H. Sharpe, D. E. Speiser, E. J. Wherry, B. A. Youngblood, D. Zehn, Defining 'T cell exhaustion'. *Nat Rev Immunol* **19**, 665-674 (2019).
5. S. J. Im, M. Hashimoto, M. Y. Gerner, J. Lee, H. T. Kissick, M. C. Burger, Q. Shan, J. S. Hale, J. Lee, T. H. Nasti, A. H. Sharpe, G. J. Freeman, R. N. Germain, H. I. Nakaya, H. H. Xue, R. Ahmed, Defining CD8+ T cells that provide the proliferative burst after PD-1 therapy. *Nature* **537**, 417-421 (2016).
6. J. C. Beltra, S. Manne, M. S. Abdel-Hakeem, M. Kurachi, J. R. Giles, Z. Chen, V. Casella, S. F. Ngiow, O. Khan, Y. J. Huang, P. Yan, K. Nzingha, W. Xu, R. K. Amaravadi, X. Xu, G. C. Karakousis, T. C. Mitchell, L. M. Schuchter, A. C. Huang, E. J. Wherry, Developmental Relationships of Four Exhausted CD8(+) T Cell Subsets Reveals Underlying Transcriptional and Epigenetic Landscape Control Mechanisms. *Immunity* **52**, 825-841 e828 (2020).
7. S. L. Park, M. M. Painter, S. Manne, V. Alcalde, M. McLaughlin, M. A. Sullivan, D. Mathew, L. Torres, Y. J. Huang, D. B. Reeg, N. R. Douek, T. Campos, M. Klapholz, M. A. Cardenas, V. Fang, S. F. Ngiow, W. Kc, R. R. Goel, A. E. Baxter, J. E. Wu, M. Tan, C. T. Berry, C. T. Ellebrecht, A. C. Huang, E. Papazian, Y. Liu, K. Rajasekaran, R. M. Brody, E. R. Thaler, D. Basu, A. Diab, J. R. Giles, E. J. Wherry, Tissue-resident exhausted and memory CD8(+) T cells have distinct ontogeny, function and role in disease. *Nat Immunol* **27**, 110-125 (2026).
8. L. Heyden, L. Rausch, M. H. Shannon, L. Dryburgh, M. L. Moreira, A. Frolov, C. M. Scheffler, M. J. van Elsas, J. Tong, O. Hidajat, S. K. M. Wijesinghe, S. Li, H. Horvatic, N. T. Huynh-Anh, C. Gago da Graca, C. Tsui, M. Kohne, D. Sommer, F. T. Wunderlich, B. von Scheidt, S. L. Park, L. K. Mackay, D. T. Utzschneider, J. Schroder, S. J. Turner, P. K. Darcy, M. D. Beyer, Z. Abdullah, A. Kallies, Transcriptional regulator SATB1 limits CD8(+) T cell population expansion and effector differentiation in chronic infection and cancer. *Nat Immunol* **26**, 2312-2327 (2025).
9. E. Fagerberg, J. Attanasio, C. Dien, J. Singh, E. A. Kessler, L. Abdullah, J. Shen, B. G. Hunt, K. A. Connolly, E. De Brouwer, J. He, N. R. Iyer, J. Buck, E. R. Borr, M. Damo, G. G. Foster, J. R. Giles, Y. H. Huang, J. S. Tsang, S. Krishnaswamy, W. Cui, N. S. Joshi, KLF2 maintains lineage fidelity and suppresses CD8 T cell exhaustion during acute LCMV infection. *Science* **387**, eadn2337 (2025).
10. J. Song, D. Cui, J. Wang, X. Qi, J. Ma, Q. Liu, J. Yang, H. Yu, L. Ye, Q. Huang, J. Li, F. Li, Targeting Mettl8-Tcf1 axis promotes CD8+ TPEX differentiation and antitumor immunity. *J Exp Med* **223**, (2026).
11. M. Ongaro, R. Thouenon, I. Crespo, A. Dumez, M. Charmoy, E. Roman Camacho, V. J. Morel, D. Cropp, E. Desponds, G. Zanette, Y. C. Wang, L. Vergili, L. Tille, I. Di Resta,

M. M. Leblond, J. Corria Osorio, P. C. Ho, W. Held, G. Verdeil, The transcription factor IRF8 drives tumor-specific exhaustion in CD8+ T cells. *J Exp Med* **223**, (2026).
12. A. C. Scott, F. Dundar, P. Zumbo, S. S. Chandran, C. A. Klebanoff, M. Shakiba, P. Trivedi, L. Menocal, H. Appleby, S. Camara, D. Zamarin, T. Walther, A. Snyder, M. R. Femia, E. A. Comen, H. Y. Wen, M. D. Hellmann, N. Anandasabapathy, Y. Liu, N. K. Altorki, P. Lauer, O. Levy, M. S. Glickman, J. Kaye, D. Betel, M. Philip, A. Schietinger, TOX is a critical regulator of tumour-specific T cell differentiation. *Nature* **571**, 270-274 (2019).
13. O. Khan, J. R. Giles, S. McDonald, S. Manne, S. F. Ngiow, K. P. Patel, M. T. Werner, A. C. Huang, K. A. Alexander, J. E. Wu, J. Attanasio, P. Yan, S. M. George, B. Bengsch, R. P. Staupe, G. Donahue, W. Xu, R. K. Amaravadi, X. Xu, G. C. Karakousis, T. C. Mitchell, L. M. Schuchter, J. Kaye, S. L. Berger, E. J. Wherry, TOX transcriptionally and epigenetically programs CD8(+) T cell exhaustion. *Nature* **571**, 211-218 (2019).
14. F. Alfei, K. Kanev, M. Hofmann, M. Wu, H. E. Ghoneim, P. Roelli, D. T. Utzschneider, M. von Hoesslin, J. G. Cullen, Y. Fan, V. Eisenberg, D. Wohlleber, K. Steiger, D. Merkler, M. Delorenzi, P. A. Knolle, C. J. Cohen, R. Thimme, B. Youngblood, D. Zehn, TOX reinforces the phenotype and longevity of exhausted T cells in chronic viral infection. *Nature* **571**, 265-269 (2019).
15. Y. Xu, Y. Shangguan, Y. M. Chuang, T. H. Chang, W. Liu, J. J. Peng, J. Garnica, L. Xie, P. C. Hsueh, M. C. Lin, Y. H. Wang, K. L. Hajdu, Y. Wu, M. Akrami, C. Wang, A. Kohl, A. Zippelius, W. Qi, M. Wang, B. R. Budiarto, S. Y. Chen, Z. Xiao, P. Vardaka, R. Roychoudhuri, Z. Bai, R. Fan, S. Carmona, Y. R. Yu, C. Scheiermann, J. Wang, P. C. Ho, Proteasome-guided haem signalling axis contributes to T cell exhaustion. *Nature* **653**, 548-557 (2026).
16. Y. Guo, Y. Q. Xie, M. Gao, Y. Zhao, F. Franco, M. Wenes, I. Siddiqui, A. Bevilacqua, H. Wang, H. Yang, B. Feng, X. Xie, C. M. Sabatel, B. Tschumi, A. Chaiboonchoe, Y. Wang, W. Li, W. Xiao, W. Held, P. Romero, P. C. Ho, L. Tang, Metabolic reprogramming of terminally exhausted CD8(+) T cells by IL-10 enhances anti-tumor immunity. *Nat Immunol* **22**, 746-756 (2021).
17. S. J. Turner, T. J. Bennett, N. L. La Gruta, CD8(+) T-Cell Memory: The Why, the When, and the How. *Cold Spring Harb Perspect Biol* **13**, (2021).
18. J. Park, P. C. Hsueh, Z. Li, P. C. Ho, Microenvironment-driven metabolic adaptations guiding CD8(+) T cell anti-tumor immunity. *Immunity* **56**, 32-42 (2023).
19. J. Linden, F. Koch-Nolte, G. Dahl, Purine Release, Metabolism, and Signaling in the Inflammatory Response. *Annu Rev Immunol* **37**, 325-347 (2019).
20. A. Manica, A. M. Da Silva, A. M. Cardoso, M. Moreno, D. B. Leal, A. Dutra Da Silva, M. R. C. Schetinger, V. M. M. Morsch, M. D. Bagatini, High levels of extracellular ATP lead to chronic inflammatory response in melanoma patients. *J Cell Biochem* **119**, 3980-3988 (2018).
21. E. K. Kaufman, T. H. Swartz, Pannexin-1-mediated ATP signaling as a driver of immune communication and chronic inflammation in HIV infection. *Front Immunol* **17**, 1836368 (2026).
22. F. Di Virgilio, D. Dal Ben, A. C. Sarti, A. L. Giuliani, S. Falzoni, The P2X7 Receptor in Infection and Inflammation. *Immunity* **47**, 15-31 (2017).
23. H. Borges da Silva, L. K. Beura, H. Wang, E. A. Hanse, R. Gore, M. C. Scott, D. A. Walsh, K. E. Block, R. Fonseca, Y. Yan, K. L. Hippen, B. R. Blazar, D. Masopust, A.

Kelekar, L. Vulchanova, K. A. Hogquist, S. C. Jameson, The purinergic receptor P2RX7 directs metabolic fitness of long-lived memory CD8(+) T cells. *Nature* **559**, 264-268 (2018).
24. H. Borges da Silva, C. Peng, H. Wang, K. M. Wanhainen, C. Ma, S. Lopez, A. Khoruts, N. Zhang, S. C. Jameson, Sensing of ATP via the Purinergic Receptor P2RX7 Promotes CD8(+) Trm Cell Generation by Enhancing Their Sensitivity to the Cytokine TGF-beta. *Immunity* **53**, 158-171 e156 (2020).
25. T. Vardam-Kaur, S. van Dijk, C. Peng, K. M. Wanhainen, S. C. Jameson, H. Borges da Silva, The Extracellular ATP Receptor P2RX7 Imprints a Promemory Transcriptional Signature in Effector CD8(+) T Cells. *J Immunol* **208**, 1686-1699 (2022).
26. J. R. Giles, S. F. Ngiow, S. Manne, A. E. Baxter, O. Khan, P. Wang, R. Staupe, M. S. Abdel-Hakeem, H. Huang, D. Mathew, M. M. Painter, J. E. Wu, Y. J. Huang, R. R. Goel, P. K. Yan, G. C. Karakousis, X. Xu, T. C. Mitchell, A. C. Huang, E. J. Wherry, Shared and distinct biological circuits in effector, memory and exhausted CD8(+) T cells revealed by temporal single-cell transcriptomics and epigenetics. *Nat Immunol* **23**, 1600-1613 (2022).
27. T. A. DePauw, K. Gai, J. Shen, N. J. Maurice, K. H. Rhee, W. J. Valente, C. H. O'Connor, W. Cui, C. Peng, S. C. Jameson, KLF2 overrides the resident memory CD8 T cell differentiation program, in opposition to KLF3. *Proc Natl Acad Sci U S A* **123**, e2533700123 (2026).
28. J. Shen, R. J. Brown, Y. Zhang, K. Gai, A. K. Brown, A. M. Bauer, A. Zhu, S. Lin, H. Niu, A. Kharel, Z. Xu, G. S. Cohen, T. A. Depauw, E. Fagerberg, G. S. Kansas, N. S. Joshi, S. C. Jameson, W. Cui, Kruppel-like factors 2 and 3 regulate T cell exhaustion by directing T cell residency and migration. *Immunity* **59**, 1287-1305 e1287 (2026).
29. N. M. Pollak, M. Hoffman, I. J. Goldberg, K. Drosatos, Kruppel-like factors: Crippling and un-crippling metabolic pathways. *JACC Basic Transl Sci* **3**, 132-156 (2018).
30. J. Zhang, S. Hashmi, F. Cheema, N. Al-Nasser, R. Bakheet, R. S. Parhar, F. Al-Mohanna, R. Gaugler, M. M. Hussain, S. Hashmi, Regulation of lipoprotein assembly, secretion and fatty acid beta-oxidation by Kruppel-like transcription factor, klf-3. *J Mol Biol* **425**, 2641-2655 (2013).
31. C. M. Carlson, B. T. Endrizzi, J. Wu, X. Ding, M. A. Weinreich, E. R. Walsh, M. A. Wani, J. B. Lingrel, K. A. Hogquist, S. C. Jameson, Kruppel-like factor 2 regulates thymocyte and T-cell migration. *Nature* **442**, 299-302 (2006).
32. J. Y. Lee, C. N. Skon, Y. J. Lee, S. Oh, J. J. Taylor, D. Malhotra, M. K. Jenkins, M. G. Rosenfeld, K. A. Hogquist, S. C. Jameson, The transcription factor KLF2 restrains CD4(+) T follicular helper cell differentiation. *Immunity* **42**, 252-264 (2015).
33. L. Douguet, S. Janho Dit Hreich, J. Benzaquen, L. Seguin, T. Juhel, X. Dezitter, C. Duranton, B. Ryffel, J. Kanellopoulos, C. Delarasse, N. Renault, C. Furman, G. Homerin, C. Feral, J. Cherfils-Vicini, R. Millet, S. Adriouch, A. Ghinet, P. Hofman, V. Vouret-Craviari, A small-molecule P2RX7 activator promotes anti-tumor immune responses and sensitizes lung tumor to immunotherapy. *Nat Commun* **12**, 653 (2021).
34. M. M. McCausland, S. Crotty, Quantitative PCR technique for detecting lymphocytic choriomeningitis virus in vivo. *J Virol Methods* **147**, 167-176 (2008).
35. L. Evgin, A. L. Huff, P. Wongthida, J. Thompson, T. Kottke, J. Tonne, M. Schuelke, K. Ayasoufi, C. B. Driscoll, K. G. Shim, P. Reynolds, D. D. Monie, A. J. Johnson, M. Coffey, S. L. Young, G. Archer, J. Sampson, J. Pulido, L. S. Perez, R. Vile, Oncolytic

virus-derived type I interferon restricts CAR T cell therapy. *Nat Commun* **11**, 3187 (2020).
36. K. M. Wanhainen, C. Peng, M. H. Zhou, B. G. Macedo, S. O'Flanagan, T. Yang, A. Kelekar, B. J. Burbach, H. Borges da Silva, S. C. Jameson, P2RX7 Enhances Tumor Control by CD8+ T Cells in Adoptive Cell Therapy. *Cancer Immunol Res* **10**, 871-884 (2022).
37. H. Borges da Silva, H. Wang, L. J. Qian, K. A. Hogquist, S. C. Jameson, ARTC2.2/P2RX7 Signaling during Cell Isolation Distorts Function and Quantification of Tissue-Resident CD8(+) T Cell and Invariant NKT Subsets. *J Immunol* **202**, 2153-2163 (2019).
38. F. Vanden Abeele, G. Bidaux, D. Gordienko, B. Beck, Y. V. Panchin, A. V. Baranova, D. V. Ivanov, R. Skryma, N. Prevarskaya, Functional implications of calcium permeability of the channel formed by pannexin 1. J Cell Biol 174, 535-546 (2006).
39. S. Xu, O. Chaudhary, P. Rodriguez-Morales, X. Sun, D. Chen, R. Zappasodi, Z. Xu, A. F. M. Pinto, A. Williams, I. Schulze, Y. Farsakoglu, S. K. Varanasi, J. S. Low, W. Tang, H. Wang, B. McDonald, V. Tripple, M. Downes, R. M. Evans, N. A. Abumrad, T. Merghoub, J. D. Wolchok, M. N. Shokhirev, P. C. Ho, J. L. Witztum, B. Emu, G. Cui, S. M. Kaech, Uptake of oxidized lipids by the scavenger receptor CD36 promotes lipid peroxidation and dysfunction in CD8(+) T cells in tumors. Immunity 54, 1561-1577 e1567 (2021).
40. F. A. Wolf, P. Angerer, F. J. Theis, SCANPY: large-scale single-cell gene expression data analysis. *Genome Biol* **19**, 15 (2018).
41. M. Evrard, E. Becht, R. Fonseca, A. Obers, S. L. Park, N. Ghabdan-Zanluqui, J. Schroeder, S. N. Christo, D. Schienstock, J. Lai, T. N. Burn, A. Clatch, I. G. House, P. Beavis, A. Kallies, F. Ginhoux, S. N. Mueller, R. Gottardo, E. W. Newell, L. K. Mackay, Single-cell protein expression profiling resolves circulating and resident memory T cell diversity across tissues and infection contexts. *Immunity* **56**, 1664-1680 e1669 (2023).
42. E. Becht, D. Tolstrup, C. A. Dutertre, P. A. Morawski, D. J. Campbell, F. Ginhoux, E. W. Newell, R. Gottardo, M. B. Headley, High-throughput single-cell quantification of hundreds of proteins using conventional flow cytometry and machine learning. *Sci Adv* **7**, eabg0505 (2021).
43. S. A. Vardhana, M. A. Hwee, M. Berisa, D. K. Wells, K. E. Yost, B. King, M. Smith, P. S. Herrera, H. Y. Chang, A. T. Satpathy, M. R. M. van den Brink, J. R. Cross, C. B. Thompson, Impaired mitochondrial oxidative phosphorylation limits the self-renewal of T cells exposed to persistent antigen. *Nat Immunol* **21**, 1022-1033 (2020).
44. R. J. Arguello, A. J. Combes, R. Char, J. P. Gigan, A. I. Baaziz, E. Bousiquot, V. Camosseto, B. Samad, J. Tsui, P. Yan, S. Boissonneau, D. Figarella-Branger, E. Gatti, E. Tabouret, M. F. Krummel, P. Pierre, SCENITH: A Flow Cytometry-Based Method to Functionally Profile Energy Metabolism with Single-Cell Resolution. *Cell Metab* **32**, 1063-1075 e1067 (2020).

Supplementary Files

This is a list of supplementary files associated with this preprint. Click to download.

- ExtendedDataFig1.pdf
- SupplementaryTable2.pdf
- SupplementaryTable1.pdf
- ExtendedDataFig5.pdf
- ExtendedDataFig8.pdf
- ExtendedDataFig7.pdf
- ExtendedDataFig3.pdf
- ExtendedDataFig9.pdf
- ExtendedDataFig2.pdf
- ExtendedDataFiguresv2.docx
- ExtendedDataFig4.pdf
- ExtendedDataFig10.pdf
- ExtendedDataFig6.pdf